SEISMIC PERFORMANCE ASSESSMENT OF STEEL CHEVRON BRACED FRAMES DESIGNED TO THE TURKISH BUILDING EARTHQUAKE CODE 2018

A Thesis

By

Mesut ADALI

Submitted to the

Graduate School of Sciences and Engineering

In Partial Fulfillment of the Requirements for

The Degree of

Master of Science

In The

Department of Civil Engineering

Özyeğin University

January 2021

SEISMIC PERFORMANCE ASSESSMENT OF STEEL CHEVRON BRACED FRAMES DESIGNED TO THE TURKISH BUILDING EARTHQUAKE CODE 2018

Approved By:

Asst. Prof. Yiğit Özçelik

Advisor

Department of Civil Engineering

Özyeğin University

Asst. Prof. Bülent Erkmen

Department of Civil Engineering

Özyeğin University

Asst. Prof. Bahadır Şadan

Deparment of Civil Engineering

MEF University

Date Approved: 18 January 2021

DEDICATION

To my father with longing and pray…

ABSTRACT

Concentrically braced frames (CBFs) are commonly preferred in high seismicity areas to provide resistance against seismic loads. After significant damages were observed in moment frames during the Northridge (1994) and Kobe (1995) earthquakes, CBFs have become more popular owing to high stiffness and strength. Thus, research has been focused on behaviour of CBFs under severe earthquakes.

One of the configurations of CBFs is chevron (or inverted-V) braced frames (IVBFs) is also used in structures because of their architectural advantages. In chevron arrangement, while one of the story braces resist compression, the other one resist tension. Chevron CBFs require special consideration in design. Because, under a lateral loading when the compression brace buckles, the downward force emerges at the midspan of the beam. This unbalanced force can lead to formation of a plastic hinge at the midspan of the beam and collapse of the structure. To avoid such an undesirable mechanism, the Turkish Building Earthquake Code 2018 (TBEC) that superseded the Turkish Earthquake Code 2007 introduced two yield mechanisms. TBEC requires the beams, columns, and connections of IVBFs to be designed to resist the axial and flexural demands obtained from two yield mechanisms.

In this study, firstly, a two-story IVBF was designed per TBEC considering new provisions and changes such as yield mechanism, earthquake ground motion intensity levels, and performance levels. Nonlinear response-history analyses were conducted to evaluate seismic performance of IVBF under ground motions. Secondly, incremental dynamic analysis (IDA) of a two-story IVBF designed to TBEC was performed. Capacity points were determined for each IDA curve and the collapse fragility curve of the frame

was obtained. Collapse margin ratio defined in FEMA P-695 was calculated. Finally, the acceptability of calculated collapse margin ratio was evaluated.

ÖZETÇE

Merkezi çaprazlı çelik çerçeveler (MÇÇÇ) sismik yüklere dayanım sağlamak için genellikle tercih edilirler. Kobe (1995) ve Northgate (1994) depremlerinde gözlemlenen önemli hasarlardan sonra, MÇÇÇler yüksek rijitlik ve dayanıma sahip olmalarından dolayı daha popüler olmuşlardır. Böylece çalışmalar MÇÇÇlerin şiddetli depremlere maruz kaldığındaki davranışlarını araştırmaya odaklanmıştır.

MÇÇÇlerin konfigürasyonlarından bir tanesi olan ters V çapraz çerçeveler mimari avantajlarından dolayı yapılarda tercih edilir. Ters V çapraz çerçevelerde, çapraz elemanlardan biri basınç kuvvetlerine dayanım sağlarken diğer çapraz eleman çekme kuvvetlerine dayanım sağlar. Ters V çapraz çerçeveler diğer çerçeve konfigürasyonlarından farklı olarak özel tasarım hususları gerektirmektedirler. Deprem kuvvetleri altında çapraz elemanların birinin burkulması durumunda kiriş orta açıklığında dengelenmemiş bir kuvvet oluşacaktır. Bu kuvvet kiriş orta açıklığında plastik mafsal oluşumuna sebebiyet vererek yapının göçmesine sebep olabilir. Bu durumundan kaçınmak için Türkiye Deprem Yönetmeliği'nin (TEC,2007) yerine kullanıma sunulan Türkiye Bina Deprem Yönetmeliği 2018 (TBDY) iki tane akma (mekanizma) durumu önermektedir. TBDY uyarınca, çerçeve elemanları olan kiriş, kolon ve çaprazların, bu iki akma durumundan elde edilen iç kuvvetlere göre dizayn edilmesi gerekmektedir.

Bu çalışmada, ilk olarak 2 katlı ters V çapraz çerçeve sistem TBDY'nin yeni önerileri de dikkate alınarak dizayn edilmiştir. Ters V çapraz çerçeve sistemin sismik performansını değerlendirmek için zaman tanım alanında doğrusal olmayan deprem hesabı yapılmıştır. Bu çalışmaya ek olarak, artımsal dinamik analiz yöntemi ile ters V çerçeve sistem üzerinde zaman tanım alanında doğrusal olmayan deprem hesabı

yapılmıştır. Elde edilen artımsal dinamik analiz eğrileri üzerinde kapasite noktaları belirlenmiş olup göçme kırılganlık eğrisi elde edilmiştir. FEMA P-595'de tanımlanan göçme marj oranı hesaplanmıştır. Son olarak hesaplanan bu göçme marj oranı değerinin kabul edilebilirliği değerlendirilmiştir.

ACKNOWLEDGMENTS

I would like to express gratitude to my advisor Dr. Yiğit Özçelik for his guidance, patience and teaching during my research. My sincere thanks also go to Dr.Bülent Erkmen and Dr. Bahadır Şadan for taking part of my thesis committee members.

I am very lucky and happy to have taken some courses from Dr. Derya Deniz and Dr. Taner Yılmaz. Especially, the courses that I have taught by Dr. Derya Deniz have inspired me in regard to basis of engineering and prompted me to do research and study deeply in new research areas.

I am also grateful for the warm friendship of my colleagues during my master`s education. Their supports in my life and research are highly appreciated. Special thanks to the administrative staff member Gizem Bakır for her support and help.

Special thanks to my family for supporting me during my all-education life. Also, I dedicated this thesis to my lovely the deceased father. I believe that his unconditional support and effort have been my motivation so far and so it shall be.

TABLE OF CONTENTS

LIST OF TABLES

LIST OF FIGURES

This page is intentionally left blank.

CHAPTER I

INTRODUCTION

1.1 Background

Since critical damages were observed in steel moment resisting frames (SMRF) after severe earthquakes such as 1994 Northridge earthquake [1], concentrically braced frames (CBFs) were started to be used in construction widely due to their high stiffness and ductility (Figure 1-1). Also, CBFs are more advantageous in constructability and cost-effective systems compared to SMRF [2]. CBFs resist lateral loads due to seismic excitation by working in truss action. In the CBFs, system absorbs earthquake energy by yielding of tension brace and buckling of compression brace.

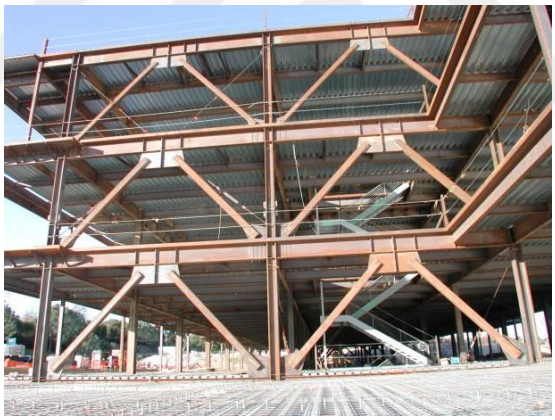

Figure 1-1: Chevron braced frame (Engelhardt, 2007)

Chevron (inverted-V) braced frames (IVBFs) are one of the configurations of the concentrically braced frames where upper ends of braces meet story beam at its mid-length as shown in Figure 1-2. In IVBFs, while one of the story braces develops tensile stress, opposite brace develops compressive stress as given in Figure 1-3.

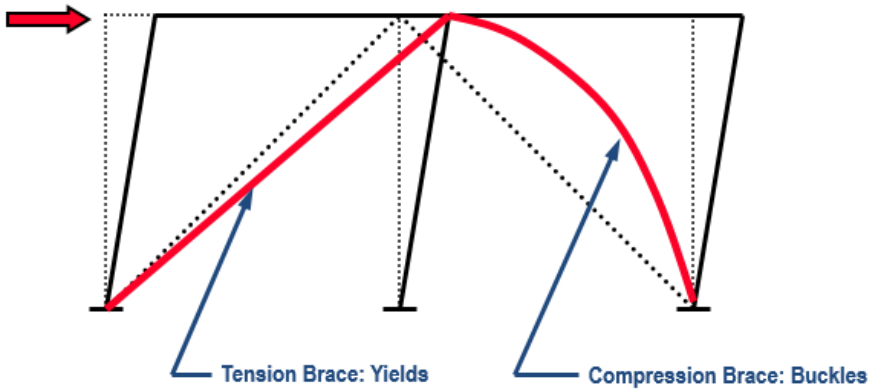

(a)

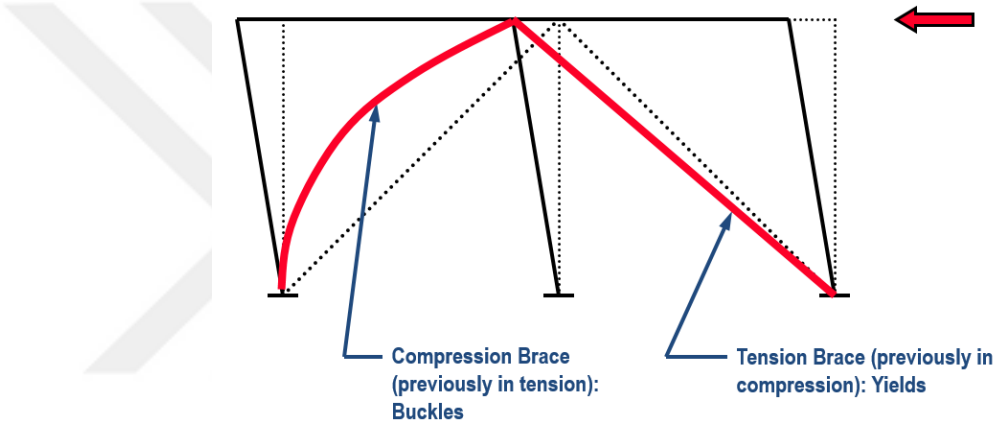

(b)

Figure 1-2 Response of chevron braced frame under a lateral loading (Engelhardt, 2007)

In case where the compression brace buckles, an unbalanced force emerges at the midspan of the beam. As reported in past experiments by Wakabayashi (1983) [3] and Fukuta et al. (1989) [4], the behavior of IVBFs is influenced by this unbalanced downward force which might cause the formation of plastic hinge at the midspan of the beam. Since this undesirable situation can lead to the collapse of the frame eventually, for the design of the IVBFs, special considerations should be taken.

1.2 Problem Statement

The main problem in IVBFs is plastic hinge formation at the midspan of the beam that might cause collapse of the structure. The Turkish Building Earthquake Code 2018 (TBEC) [5] introduced two yield mechanisms (Figures 1-3b and 1-3c) for concentrically braced frames (CBFs) given in Figure 1-3a. In the first yield mechanism (Figure 1-1b), all braces are assumed to resist forces corresponding to their expected strength in tension or in compression. The expected brace strength in tension is given as $R_yF_yA_g$ where R_yF_y is the expected yield stress and A_g is the gross cross-sectional area. The expected brace strength in compression is given as $1.14F_{cre}A_g$ where F_{cre} is determined from Chapter 8 of the Turkish Specification of Steel Structures 2016 (TSSS) [6] using the equations for the critical stress, F_{cr}, except that R_yF_y is used in lieu of the minimum yield stress, F_y. In the second yield mechanism (Figure 1-1 c), all braces are assumed to resist forces corresponding to their expected strength in tension or their expected post-buckling strength. The expected post-buckling brace strength is assumed to 30% of the expected brace strength in compression. TBEC [5] requires the beams, columns, and connections in IVBFs to be designed to resist the axial and flexural demands resulting from these two yield mechanisms to preclude potential collapse. Note that such yield mechanisms were not covered, and these capacity design principles were not adopted for CBFs in the previous edition of TBEC, namely, the Turkish Earthquake Code 2007 (TEC) [7]. Consequently, IVBFs designed per TBEC [5] are expected to have heftier members (especially the beams of IVBFs) compared to TEC [7].

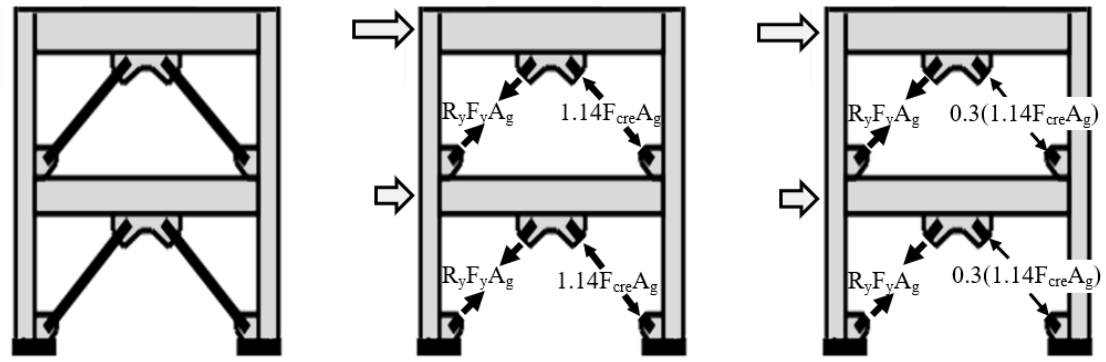

Figure 1-3: IVBF: (a) Elevation view, (b) yield mechanism 1, (c) yield mechanism 2

In addition to the introduction of the aforementioned yield mechanisms, there are a significant number of changes in TBEC [5] with respect to TEC [7]. One of the notable changes is the introduction of earthquake ground motion intensity levels. In TEC [7], there was only one ground motion intensity level considered, namely, design basis earthquake, that corresponds to an earthquake with a 10% probability of exceedance in 50 years, in other words, earthquake with a return period of 475 years. In TBEC, there are four ground motion intensity levels, namely, DD1, DD2, DD3, and DD4 that correspond to 2%, 10%, 50%, and 68% probability of exceedance in 50 years, respectively. Except for some special cases such as tall buildings and important facilities to be used post-earthquakes such as hospitals and fire stations, the earthquake loads for the design of new buildings are determined per DD2 that can be considered as the design basis earthquake for TBEC [5]. Consequently, it can be inferred that the design approach is similar in terms of uniform seismic hazard levels. However, TBEC [5] sets discrete performance levels for the defined ground motion intensity levels (such levels were not covered in TEC). In Chapter 5C, TBEC [5] introduces deformation limits for structural components for each performance target, namely, limited damage (SH), controlled damage (KH), collapse prevention (GO). These deformation limits are given as plastic

rotations for beams and columns and as plastic axial deformations (elongation or shortening) for braces.

1.3 Research Objectives

The main aim of the study is to assess the seismic performance of chevron braced frames designed to TBEC 2018 [5] as the code has been recently introduced and there are only limited number (or no study) on this topic. For this purpose, following objectives are undertaken;

- To evaluate the performance of IVBF per the deformation limits given in TBEC,
- To assess the collapse fragility of IVBFs using the incremental dynamic analyses.

1.4 Organization of the Thesis

This thesis is consisted of seven chapters.

Chapter 1 presents an introduction about the background and objectives of this study.

Chapter 2 includes a literature review on experimental and analytical studies on chevron braced steel frames.

Chapter 3 explains the developed spreadsheet and methodology of the building design in this study.

Chapter 4 includes description of numerical modeling and validation for chevron braced frame generated with developed spreadsheet.

In Chapter 5, collapse assessment of study by using incremental dynamic analysis on chevron braced frame is presented.

In Chapter 6, seismic performance assessment of chevron braced frame designed to the Turkish Building Earthquake Code is presented.

Chapter 7 gives the conclusions of the study and recommendations for future works.

CHAPTER II

LITERATURE REVIEW

In this chapter, a brief summary of experimental and analytical studies on chevron braced frames are presented.

2.1 Experimental Studies

Sen et al. [8] conducted an experimental program on the four two-story chevron braced frames at the National Center for Earthquake Engineering (NCREE). The four specimens have story heights of 3297 mm and bay width of 6286 mm. The details of four specimens tabulated in Table 2-1.

Table 2-1: Geometry and members of test specimens [8]

Test Number	Specimen Name	Story	Story Height (mm)	Beam Shape	Brace Shape
1	TNCBF1-N-HSS	1	3297	W16x45	HSS7x7x1/4
		2	3297	W24x94	HSS7x7x1/4
2	TNCBF1-R-HSS	1	3297	W16x45	HSS5x5x3/8k
		2	3297	W24x94	HSS7x7x1/4
3	TNCBF1-R-WF	1	3297	W16x45	H175x175x7.5x11
		2	3297	W24x94	HSS7x7x1/4
4	TNCBF2-D-HSS	1	3297	W16x45	HSS5x5x3/8
		2	3297	W24x94	HSS5x5x3/8

The first specimen represented a non-ductile chevron braced frame with a beam that does not remain elastic in post-buckling condition. The second and third specimens examined repair strategies for the first specimen by replacing the braces and gusset plates of the first story. These specimens had seismically compact braces.

As a result of this test, it was concluded that:

- Non-compact HSS braces have very low ductility fracture immediately after buckling.

The experimental research that tested single-story single-bay chevron braced frames was conducted by Terpstra [9] at the University of Washington Structural Research Lab. The study aimed to investigate the effect of beam yielding under the unbalanced load obtained from post-buckling condition.

Beam section was the only variable in the tests. There specimens tested in this study had the same dimensions and connection details as shown in Figure 2-1. The first specimen satisfied all code provisions and also the beam has ability of resisting unbalanced load that arise from buckled compression brace strength and tension brace strength.

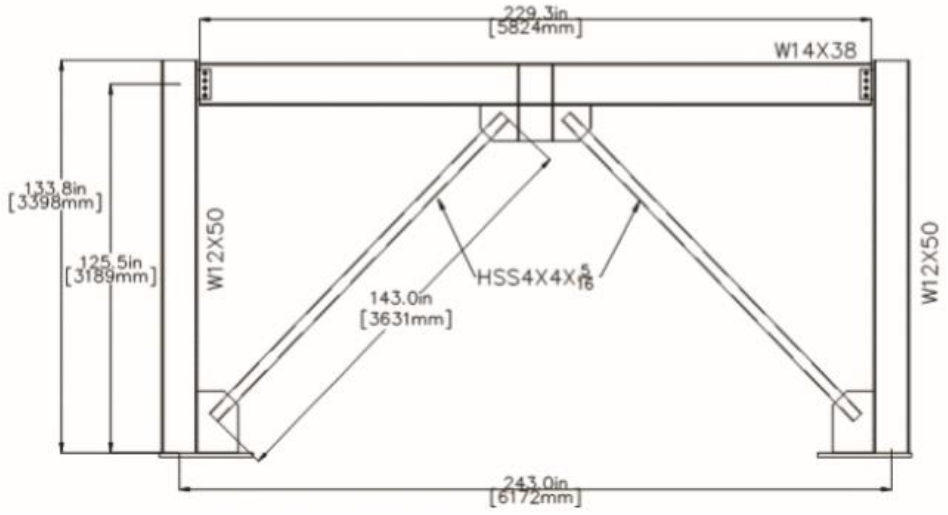

Figure 2-1: Typical test specimen [13]

Quasi-static cyclic displacement protocol to large drift demands was applied to specimen. After observing fracture of both braces, post-fracture cycles were run to determine the residual lateral resistance of the frame.

In test 1 for the first specimen, the beam yielding was not observed and there was minimal plastic deformation. A large out of plane deformation leads to brace fracture.

In test 2 for the second specimen, the beam started to yield at 1.4% story drift and continued plastic deformation by the end of the test. The braces achieved 73% of their tensile capacity and yielding was not observed.

In test 3 for the third specimen, the braces achieved 48% of their tensile capacity or 112% of the expected compressive capacity. Severe deformation caused the brace fracture.

As a result of these tests, it can be concluded that:

- Developed inelastic story drift before brace fracture was bigger for chevron braced frames with beam yielding compared to chevron braced frames without beam yielding.
- The lateral resistance of the frame decreases with beam yielding.
- As expected, vertical deflections of the beam increase with deteriorated beam strength.

2.2 Numerical Studies

Past research on analytical models of steel braces gives three types of modelling categories: (1) phenomenological, (2) beam-column elements with several approaches to account for the interaction between bending moment and the axial force and (3) three-dimensional finite element models.

The brace performs truss action with hysteretic behaviour that simulate the experimental results in the phenomenological models. These models are considered as computationally efficient and the simplest. In this approach, model should be calibrated

with experimental data. These models have been utilized in several studies (Ikeda et al. 1984; Khatib et al. 1988; Zayas et al. 1980).

Three-dimensional finite element models obtain the hysteresis behaviour of brace from the nonlinear material response by using large deformation theory. Since these models are complexity and computationally expensive, they are not preferred in applications [5].

Intensive research (Ikeda and Mahin 1986) has been conducted on modelling brace with beam-column elements. These models are utilized linear elastic beam-column elements with an inelastic hinge at mid-length of the brace. To account for interaction between bending moment and axial force, distributed inelasticity element with plasticity models have been used recently. A geometric stiffness matrix was combined with material stiffness matrix. The validation of the model by using experimental results gave good correlations under tension forces, however correlations did not demonstrate reasonable accuracy in the compressive range.

Uriz et al. [10] were conducted a research to show behaviour of inelastic beam-column element in the model of steel brace with the OpenSees [10] computational framework. Thorough the parametric study conducted with the structural model given in Figure 2-2, effect of modelling parameters on the analytic hysteretic response of the steel brace was studied.

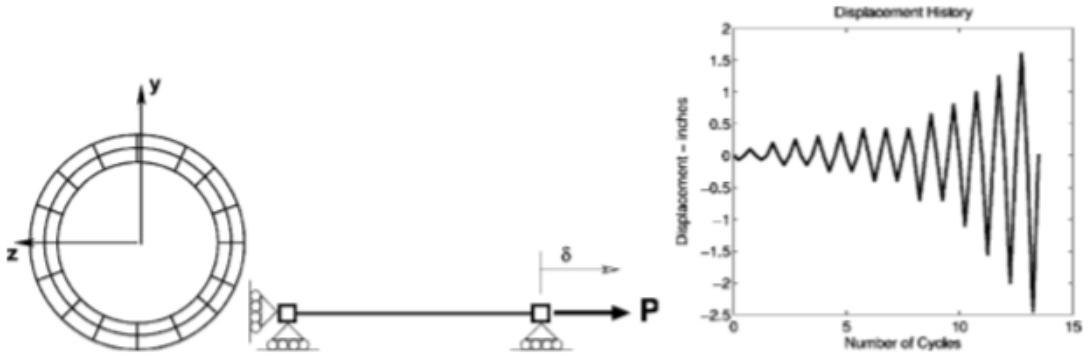

Figure 2-2: Structural model geometry used in study with displacement history [5]

The strut tests results obtained from Black et al. [11] were used for comparison. The strut cross section was 4 in. steel pipe that has yield strength of 24 ksi (165 MPa). To observe local deformations and strains in the brace, the brace should be subdivided into more than two elements. It is needed to add imperfection to geometry of analytical model of the brace for triggering buckling of brace under axial loads. Initial camber is between 0.01% and 3% of the brace length at the mid-length of the brace. The effect of imperfection on buckling behaviour of the brace under compression forces is given in Figure 2-3 (a). To simulate the initial camber more accurately, brace is divided into four elements. It can be stated that buckling load is affected by value of maximum initial camber displacement. For the initial camber value of 0.01% to 1%, essential reduction in buckling load is observed. Hysteretic response of the brace given in Figure 2-3 (b) is not very sensitive to maximum initial camber value. Results of hysteretic behaviour of the brace and experimental results given in Figure 2-6 match good. So, the numerical model is able to capture the initial buckling load, post-buckling behaviour of the brace. As a conclusion, from the results of numerical model and experiment, initial camber of 0.01% of brace length is in good agreement with the buckling load observed in the test.

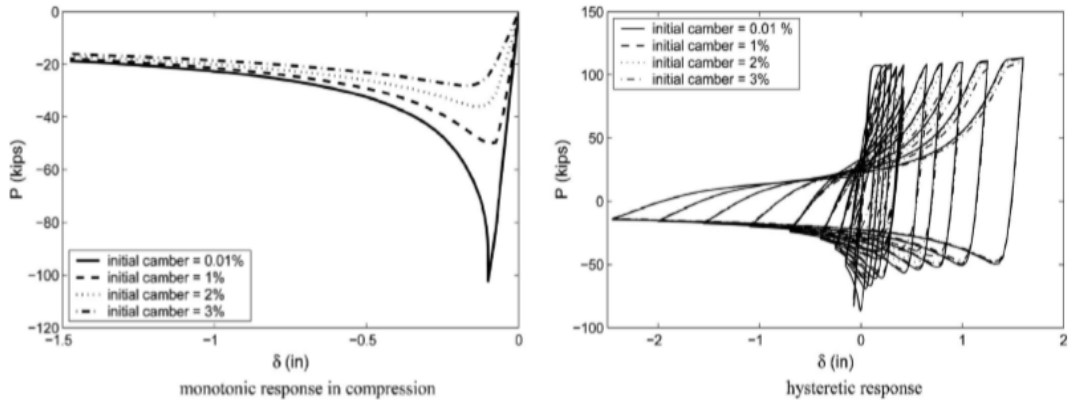

a) b)

Figure 2-3: Effect of initial camber on behaviour of strut [10]

Figure 2-4 depicts the influence of number of integration points in an element for the hysteretic displacement response of the brace under axial loading. The results of the study suggest that three Gauss integration points are enough to incorporate the hysteretic buckling behavior of the brace in modelling.

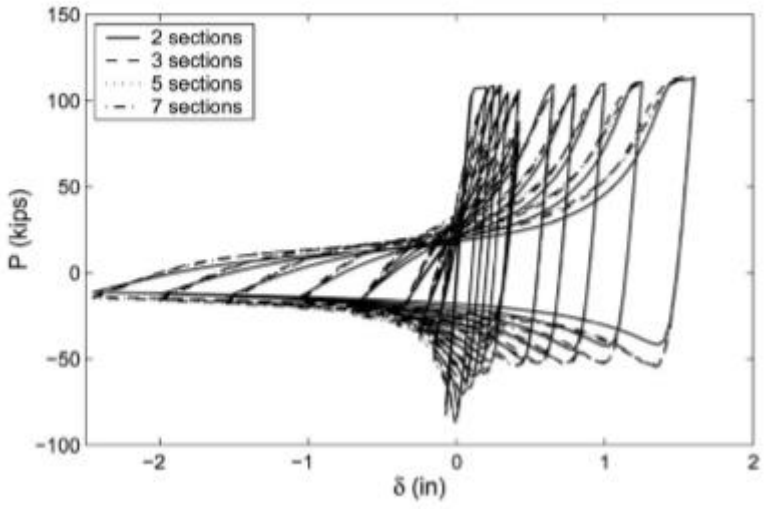

Figure 2-4: Effect of number of integration points on hysteretic behaviour of struts [10]

Uriz et al. [10] conducted a correlation studies with the past experimental results for four different cross-sections given in Figure 2-5. Two inelastic beam-column elements and three Gauss-Lobatto integration points in each element were used in the numerical

model. At the mid-length of the brace, 0.05% of the brace length was considered. Menegotto-Pinto material model [12] was assigned to structural steel. Figure 2-6 and Figure 2-7 illustrate the experimental and numerical results of hollow struts for compact and non-compact sections, respectively.

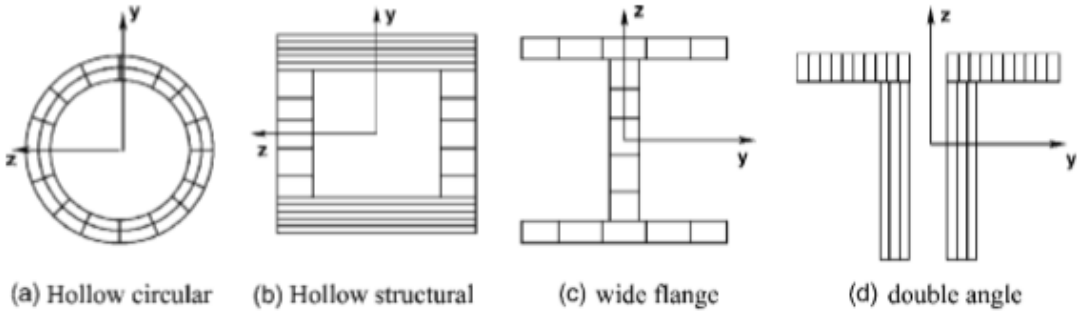

Figure 2-5: Fiber discretization of different cross-section for correlation studies [10]

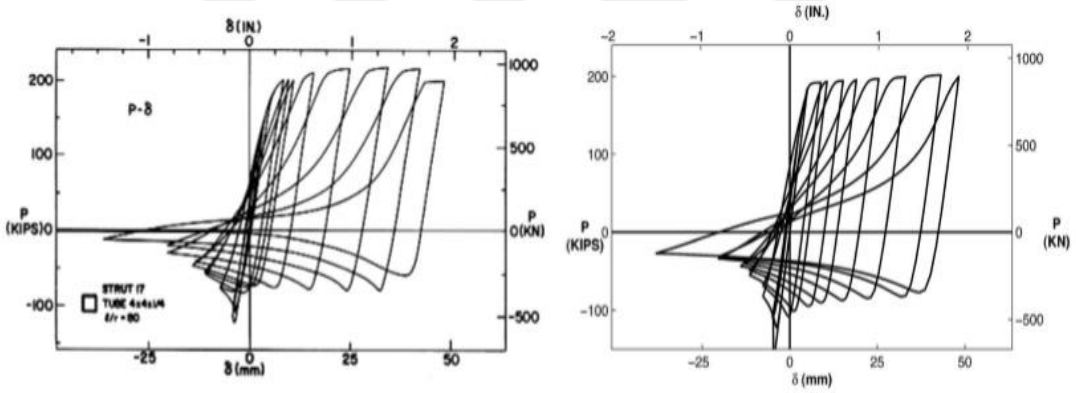

(a) Experimental results of Black et al. 1980

(b) numerical results

Figure 2-6: Hysteretic behavior correlation of HSS 4X4X1/4 strut [11]

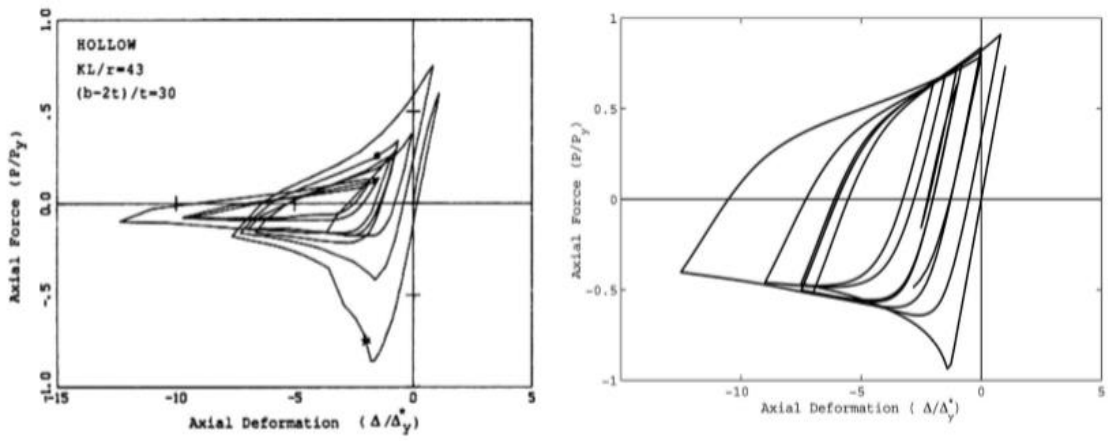

(a) Experimental results of Lee and Goel, 1987

(b) Numerical results

Figure 2-7: Hysteretic behavior correlation of HSS 4X4X1/8 strut [13]

The excellent agreement in analytical and experimental results shows that the numerical model is capable of capturing the hysteretic behaviour of struts with compact cross-sections. With the results in good agreement, the insignificant role of local buckling in compact struts with respect to global hysteretic response of the brace was proved. For the case where local buckling is important as reported in the experimental studies of Lee and Goel (1987) [7], the numerical model capture accurately buckling and tensile strength of the strut. However, it does not represent the post-buckling behaviour of the strut due to assumption that cross-sections retain their original shape.

A research conducted by Hsiao et al. [14] for the establishment of a modeling approach that could predict the seismic performance of special concentrically braced frames (SCBFs) more accurately. The important thing to model the post-buckling behaviour of the SCBFs is the capability of brace model to capture the brace behaviour adequately, including the failure mode of brace fracture. The concentration of the large strains and deformation at the mid-length of the brace brings about the brace fracture. The research aims to develop a practical line-element model to be used in nonlinear

simulations. The line-element brace model and fracture model behaviour are given in Figure 2-8.

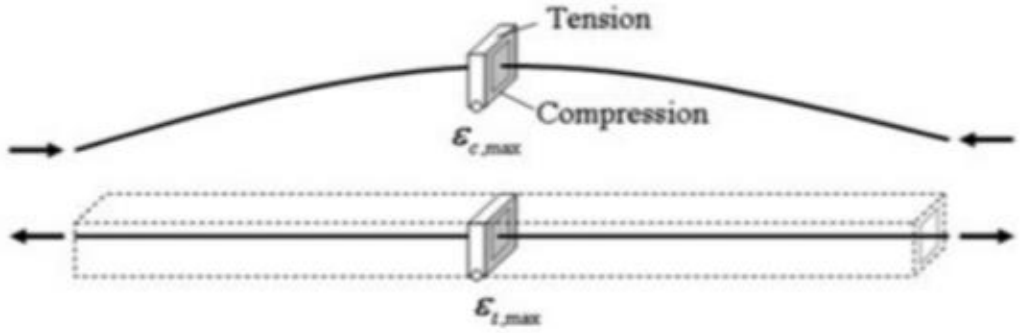

(a)

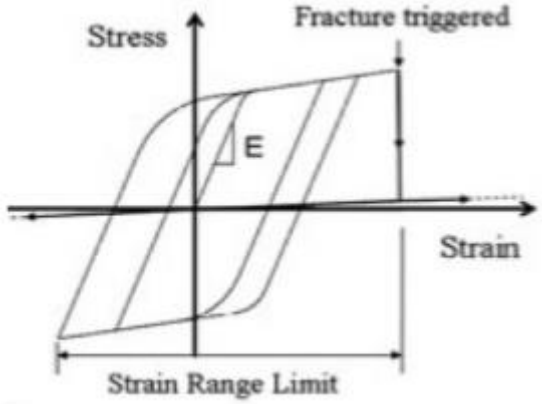

(b)

Figure 2-8: (a) Brace element fracture model with fiber section (b) Stress-strain relationship for the fracture material model [14]

The model was validated and compared to several numerical models for simulating brace fracture. Authors concluded that the model is able to simulate brace fracture accurately.

A comprehensive analytical study to investigate the behaviour of chevron braced frames was conducted by Khatib et al [15]. Six-storey building model was used in the

study. The objectives of the study are to improve the seismic response of chevron braced frame considering different configurations and various methods. As a result of nonlinear quasi-static analyses, inelastic brace behaviour is controlled by brace slenderness and relative beam stiffness. Nonlinear response analyses conducted on chevron braced frames to examine the effects of variations in these parameters. It was concluded that chevron braced frames with a very slender braces and stiff beams gives better hysteretic behavior, but caused large compressive forces to the columns. Study recommended that investigation on dynamic force redistribution in chevron braced frames should be studied. It was underlined that members of the frame should be capacity-designed.

Remennikov et al. [16] conducted a research on seismic performance of chevron braced frames with a special consideration for brace behaviour and story beams. Authors stated that chevron braced frames might perform unfavourable failure modes under severe earthquakes, therefore seismic design consideration should be taken into account to provide good inelastic seismic performance of chevron braced frames. Results of past analytical and experimental studies have shown that the seismic behaviour of the chevron braced frames are affected largely from the ratio of the beam moment resistance to brace resistance in tension. A numerical study was performed to evaluate the seismic performance of three different chevron braced frames. Each two-storey chevron braced frames was subjected to the near-field type ground motions.

As a result of this study, design rules for ordinary chevron braced frames give result a frame that is unable to resist earthquake forces. From the results obtained from this study, authors set forth a design approach, considering 80% of the yield strength of the tensile braces in the design of the beams and suggested that this approach improves seismic performance of chevron braced frames.

CHAPTER III

DEVELOPMENT OF A DESIGN SPREADSHEET FOR CHEVRON BRACED FRAMES

3.1 Methodology

Turkish Building Earthquake Code 2018 (TBEC) [5] and Turkish Specification of Steel Structures (TSSS) [6] were used to design the chevron braced frame. In the design of the chevron braced frame, seismic parameters and rules were obtained from TBEC [5] and strengths of steel elements were calculated according to TSSS [6]. Design of frame elements were conducted according to approach given in TBEC [5]. In this approach, two mechanism are considered. For the first yield mechanism, braces have their expected strength in tension or compression. In the second yield mechanism, while tension braces have their expected strength, compression braces have 30% of the expected brace strength which is post-buckling strength of the compression brace. The beams and columns of chevron braced frame were designed to resultant demands obtained from two yield mechanism.

In yield mechanism I, the expected compression strength is given as $1.14F_{cre}A_g$ where F_{cre} is calculated from TSSS [6]. For calculating F_{cre}, R_yF_y where R_y is the expected material strength factor is used instead of F_y. The expected brace strength in tension is calculated with $R_yF_yA_g$ where Ag is the gross cross-sectional area. In yield mechanism II, while expected tensile strength is calculated with $R_yF_yA_g$ again, expected compressive strength is calculated with $0.3(1.14F_{cre}A_g)$.

As a part of this study, an excel spreadsheet was developed to design the chevron braced frame according to TBEC [5] and TSSS [6]. In the design procedure, members of the frame are determined such that they satisfy the seismic limits given in TBEC in

addition to having adequate strength to resist forces obtained from two yield mechanism. As required by capacity design procedure, firstly braces are determined for the earthquake loads on the frame. Expected brace strengths given in two yield mechanism are calculated and these forces transferred to beams and columns to be designed. Finally, the lightest sections for the braces, beams and columns are determined.

3.2 Seismic Design of Building

For the design of the CBF, firstly, building information is introduced to design sheet such as number and height of bays and storeys. For the strength calculations, material strength (F_y) and modulus of elasticity (E) are provided in the sheet given in Figure 3-1. In order to compute the earthquake parameters and loads, spectral parameters for the short period (S_s) and 1 s period (S_1) that obtained from the Turkish Seismic Hazard Maps of AFAD [17] are entered. For the given soil class, design spectral parameters (S_{DS} and S_{D1}) are calculated automatically by using local soil factors (F_s and F_1) given in TBEC [5]. Accordingly, corner periods (T_A and T_B) are calculated as:

$$T_A = 0.2\frac{S_{D1}}{S_{DS}} \tag{3-1}$$

$$T_B = \frac{S_{D1}}{S_{DS}} \tag{3-2}$$

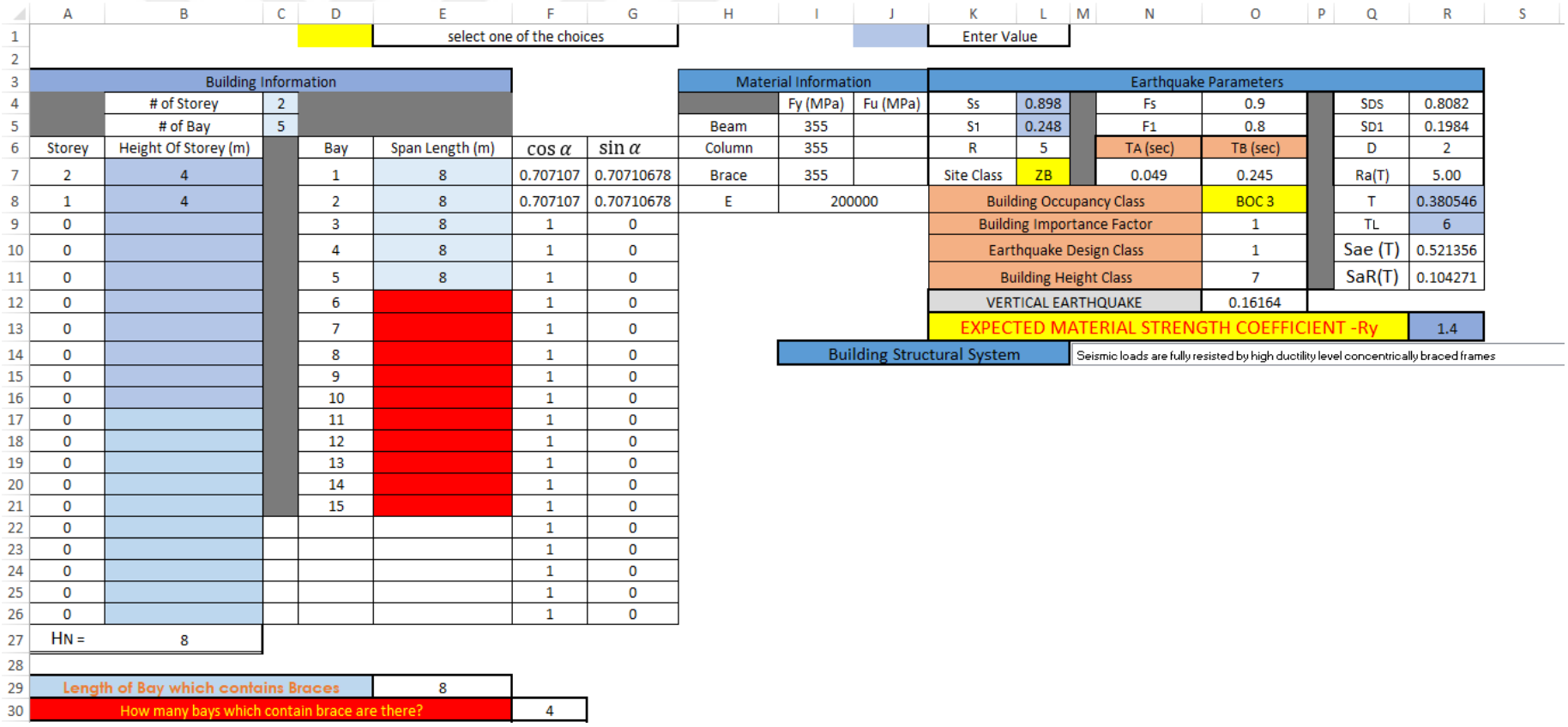

				select one of the choices						Enter Value										
Building Information							Material Information			Earthquake Parameters										
	# of Storey	2						Fy (MPa)	Fu (MPa)	Ss	0.898		Fs	0.9		SDS	0.8082			
	# of Bay	5					Beam	355		S1	0.248		F1	0.8		SD1	0.1984			
Storey	Height Of Storey (m)		Bay	Span Length (m)	cos α	sin α	Column	355		R	5		TA (sec)	TB (sec)		D	2			
2	4		1	8	0.707107	0.70710678	Brace	355		Site Class	ZB		0.049	0.245		Ra(T)	5.00			
1	4		2	8	0.707107	0.70710678	E	200000		Building Occupancy Class				BOC 3		T	0.380546			
0			3	8	1	0				Building Importance Factor				1		TL	6			
0			4	8	1	0				Earthquake Design Class				1		Sae (T)	0.521356			
0			5	8	1	0				Building Height Class				7		SaR(T)	0.104271			
0			6		1	0				VERTICAL EARTHQUAKE				0.16164						
0			7		1	0				EXPECTED MATERIAL STRENGTH COEFFICIENT -Ry							1.4			
0			8		1	0				Building Structural System				Seismic loads are fully resisted by high ductility level concentrically braced frames						
0			9		1	0														
0			10		1	0														
0			11		1	0														
0			12		1	0														
0			13		1	0														
0			14		1	0														
0			15		1	0														
0					1	0														
0					1	0														
0					1	0														
0					1	0														
0					1	0														
HN =	8																			
Length of Bay which contains Braces				8																
How many bays which contain brace are there?					4															

Figure 3-1: Building information section

After selecting building occupancy class, building importance factor (I), earthquake design class and building height class according to tables given in TBEC [5], equivalent seismic load method is conducted to compute lateral loads on each story of the chevron braced frame. In this method, total seismic load (base shear force) is distributed to the each floor levels. Total equivalent seismic load is calculated as:

$$V_{tE} = m_t S_{aR} T_p \geq 0.04 m_t I S_{DS} g \tag{3-3}$$

Where m_t is the total mass of the building, S_{aR} is reduced design spectral acceleration and T_p is the fundemental period of the structure. After determining response modification factor (R) and overstrength factor (D) for the given structural system, seismic load reduction factor (R_a) and S_{aR} are computed as:

$$\begin{aligned} R_a(T) &= \frac{R}{I} && T > T_B \\ R_a(T) &= D + \left(\frac{R}{I} - D\right)\frac{T}{T_B} && T \leq T_B \end{aligned} \tag{3-4}$$

$$S_{aR}(T) = \frac{S_{ae}(T)}{R_a(T)} \tag{3-5}$$

where $S_{ae}(T)$ is the elastic design spectral acceleration given in TBEC [5].

In order to calculate equivalent seismic load, fundamental period of the structure (T_p) is necessary. Therefore, T_p is determined from approximate fundamental period (T_{pA}) equation given in TBEC [5]. This equation is applicable for the buildings that satisfy certain conditions such as earthquake design class and building height class.

$$T_{pA} = C_t \, {H_N}^{3/4} \tag{3-6}$$

where C_t is 0.08 for steel braced frames and H_N is total height of the structure.

Gravity loads for the members of the frame is calculated by tributary area method. In the design sheet, location of the chevron braced bays is selected to run tributary area method accurately. After conducting equivalent seismic load method, earthquake loads are assigned to corresponding stories as shown in Figure 3-3. Braces are designed to resist these lateral loads. Moreover, braces are selected to satisfy slenderness ratio limits of TBEC [5]. For square hollow structural sections, width/thickness ratio is limited to $0.55\sqrt{E/F_y}$. After determining brace section, expected brace strength in tension or compression are calculated and these forces are transferred to columns and beams. To calculate the design forces of the braces, columns and beams, the equations (3-1) to (3-5) are used associated with internal forces of braces given in Figure 3-4 where *L* is the beam span length.

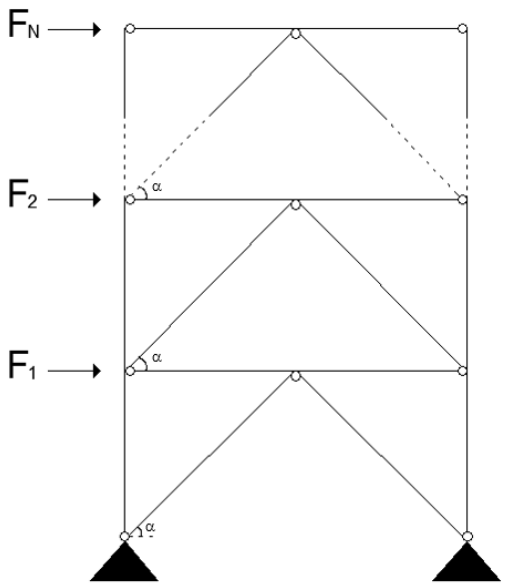

Figure 3-2: Earthquake loads acting on a chevron braced frame

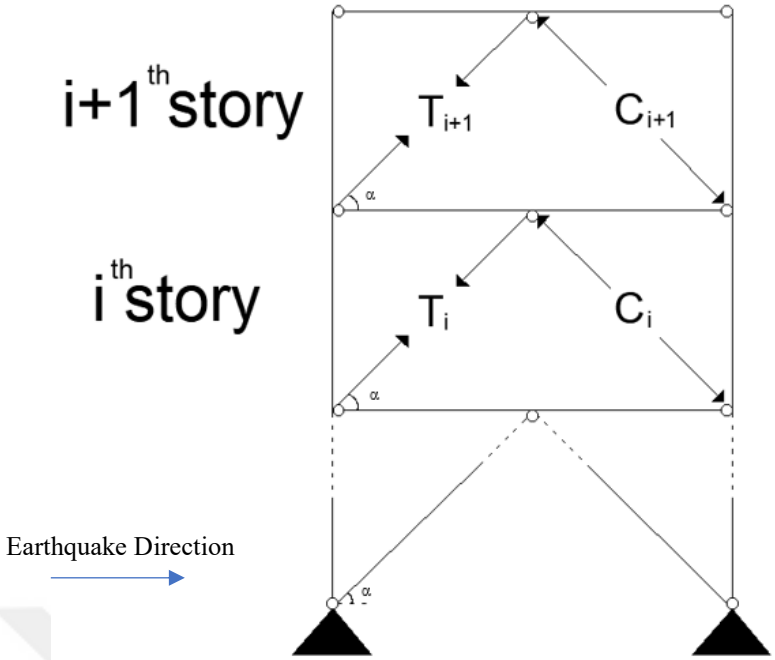

Figure 3-3: Internal forces of braces

$$T_i = C_i = \frac{\sum_{k=i}^{no.of\ stories} F_i}{2\cos\alpha} \tag{3-1}$$

$$M_{beam_i} = \frac{(T_{expected_i} - C_{expected_i})\sin\alpha\, L}{4} + \text{moment due to gravity loads} \tag{3-2}$$

$$V_{beam_i} = \frac{(T_{expected_i} - C_{expected_i})\sin\alpha}{2} + \text{shear due to gravity loads} \tag{3-3}$$

$$P_{beam_i} = (T_{expected_i} + C_{expected_i})\cos\alpha - (T_{expected_{i+1}} + C_{expected_{i+1}})\cos\alpha + axial\ load\ due\ to\ \text{gravity loads} \tag{3-4}$$

$$P_{column_i} = V_{beam_i} + P_{column_{i+1}} + T_{expected_{i+1}}\sin\alpha \tag{3-5}$$

To design the columns and beams, gravity loads and earthquake loads are combined with the following load combinations given in TSSS [6]:

$$
\begin{aligned}
&1-1.4G\\
&2-1.2G+1.6S\\
&3-1.2G+1.6Q+0.5S\\
&4-1.2G+1.6S+Q\\
&5-1.2G+Q+0.5S\\
&6-1.2G+Q+0.2S+E\\
&7-0.9G+E
\end{aligned}
\tag{3-7}
$$

where G is dead loads, S is snow loads, Q is live loads and E is earthquake loads. Also, vertical earthquake load effects are considered as following provided that certain conditions given in TBEC [5] are satisfied:

$$E_d = \frac{2}{3} S_{DS} G \tag{3-8}$$

Since the connections of columns are pin, although columns are continuous along the building height, moment demands are ignored. Therefore, columns are designed as a axial load carrying member. The beams are designed to resist the interaction of axial force (P_u) and moments (M_u) demands obtained from load combinations. The flexural strength was governed by the plastic capacity of the beam sections as it was assumed that proper lateral bracing in accordance with TBEC [5] was provided to prevent the lateral-torsional buckling.

In TBEC [5], for the flanges of the columns and beams, slenderness ratio (b/t) is limited to $0.30\sqrt{E/F_y}$. For the webs of the columns and beams, web height/web thickness ratio is limited to certain values given in TBEC [5]. In the design sheet, all of these seismic limits given in TBEC [5] are satisfied for the members of the frame. Calculations examples from developed design spreadsheet for the braces, columns and beams are given in Figure 3-5, Figure 3-6 and Figure 3-7, respectively.

U V W X Y Z AA AB AC AD AE AF AG AH AI AJ AK AL AM AN AO AP AQ AR

	LOADS					
	G	Q	Q_k	S	-	
	5	2	2			kPa
distributed load on beams	15	6	6	0		kN/m
point loads on columns	60	24	24	0	0	kN
	WEIGHT ON TOP FLOOR				6720	kN
	WEIGHT ON OTHERS FLOOR				6720	kN

Earthquake Loads Calculations

Length of Floor in X Direction	40	m	C_T	0.08		
Length of Floor in Y Direction	30	m	T_{pA}	0.380546277		
Floor Area	1200	m^2	ΔF_{Nx}	21.02106495		
			V_{tE}	1401.40433	>	434.48832

Story	mi	Hi	mi*Hi	∑ mi*Hi	(Vtx-ΔFNx)/Σ (mi *Hi)	FiEx	VtE
2	685.0153	8	5480.122	8220.183	0.167926089	920.2555	941.2766
1	685.0153	4	2740.061	8220.183	0.167926089	460.1278	1401.404
0	0	0	0	0	0	0	0
0	0	0	0	0	0	0	0
0	0	0	0	0	0	0	0
0	0	0	0	0	0	0	0
0	0	0	0	0	0	0	0
0	0	0	0	0	0	0	0
0	0	0	0	0	0	0	0
0	0	0	0	0	0	0	0
0	0	0	0	0	0	0	0
0	0	0	0	0	0	0	0
0	0	0	0	0	0	0	0
0	0	0	0	0	0	0	0
0	0	0	0	0	0	0	0
0	0	0	0	0	0	0	0
0	0	0	0	0	0	0	0
0	0	0	0	0	0	0	0
0	0	0	0	0	0	0	0
0	0	0	0	0	0	0	0
m_t	1370.031						

Figure 3-4: Calculation of earthquake loads

BRACE DESIGN																						
					SLENDERNESS CHECK				Ductility Option:			High-Ductility Level Members	1							1		
Story	Section ID	Section Name	Length (m)	W (kg/m)	b/t	0.55*(E/Fy)^0.5	CHECK	r (mm)	A_g	$\frac{KL}{r}$	KL/r<200	$4.71\sqrt{\frac{E}{F_y}}$	Buckling Type	F_e (N/mm^2)	F_{cr} (N/mm^2)	Ø Pn (kN)	P_u (kN)	CHECK	SELECTED SECTION FOR DESIGN	Pn/Pu	CapRatio
2	91	HSS4X4X.313	5.6568542	22	10.7	13.05459824	OK!	37.8	2650	149.6522	OK!	111.7948322	Elastic Buckling	88.1380347	77.2970564	184.3535	183.0353	OK!	HSS4X4X.313	1.007202	0.99285
1	98	HSS4-1/2X4-1/2X.313	5.6568542	25.2	12.5	13.05459824	OK!	43.2	3020	130.9457	OK!	111.7948322	Elastic Buckling	115.119066	100.959421	274.4077	272.5092	OK!	HSS4-1/2X4-1/2X.313	1.006967	0.993081

Figure 3-5: Design examples of braces from developed design spreadsheet

COLUMN DESIGN																					PLEASE SELECT SECTION TYPE			
					SLENDERNESS CHECK								Ductility Option:	High-Ductility Level Members	1						HE M			9
Story	Section ID	Section Name	Length (m)	W (kg/m)	b/t	0,30*(E/Fy)^0,5	CHECK	Ca	h/tw	THRESHOLD	1,49*(E/Fy)^0,5	CHECK	r (mm)	A_g (mm^2)	$\frac{KL}{r}$	$4.71\sqrt{\frac{E}{F_y}}$	Buckling Type	F_e (N/mm^2)	F_{cr} (N/mm^2)	Ø Pn (kN)	P_u (kN)	CHECK	SELECTED SECTION FOR DESIGN	Pn/Pu	CapRatio
2	2	HE 120 M	4	52.1	3	7.120689949	OK!	0.8846746	5.92	37.381263	35.36609341	OK!	32.5	6641	123.077	111.7948	Elastic Buckling	130.3096206	114.281537	683.049	604.276	OK!	HE 120 M	1.13036	0.88467
1	4	HE 160 M	4	76.2	3.6087	7.120689949	OK!	0.8811584	7.42857	37.445525	35.36609341	OK!	42.6	9705	93.8967	111.7948	Inelastic Buckling	223.887041	182.811498	1596.77	1407	OK!	HE 160 M	1.13487	0.88116

Figure 3-6: Design examples of columns from developed design spreadsheet

BEAM DESIGN																																		
												SLENDERNESS CHECK								Ductility Option :	High Ductility Level Members	1							PLEASE SELECT SECT			
Story	Section ID	Section Name	Length (m)	Ix	Zx	rts	J	Sx	Ho	ry	W (kg/m)	b/t	0,30*(E/Fy)^0,5	CHECK	Ca	h/tw	THRESHOLD	1,49*(E/Fy)^0,5	CHECK	r (mm)	A_g (mm^2)	$\frac{KL}{r}$	$4.71\sqrt{\frac{E}{F_y}}$	Buckling Type	F_e (N/mm^2)	F_{cr} (N/mm^2)	Ø Pn (kN)	L_b (mm)	L_p	L_r	Mn (kNm)				
2	17	HE 500 M	8	1619000000	7094000	147.5791472	15390000	6180000	484	74.6	270	3.825	7.120689949	OK!	0.110417885	18.57142857	52.18072094	35.36609341	OK!	216.9	34430	36.88336	111.7948322	Inelastic Buckling	1451.004875	320.4467398	9929.6831	0	3116.394	24534.11	2266.533				
1	18	HE 550 M	8	1980000000	7933000	153.7316557	15540000	6923000	532	73.5	278	3.825	7.120689949	OK!	0.109934384	20.85714286	52.20686943	35.36609341	OK!	236.4	35440	33.84095	111.7948322	Inelastic Buckling	1723.632647	325.6792526	10387.865	0	3070.442	23557.27	2534.5935				

Figure 3-7: Design examples of beams from developed design spreadsheet

CHAPTER IV

NUMERICAL MODELING OF THE CHEVRON BRACE FRAME AND VALIDATION

4.1 Numerical Modelling

Numerical model of IVBFs is generated in OpenSees [18] computational framework. A leaner column is added to the frame to take into consider P-Δ effects due to rest of the building. To represent the post-buckling behaviour of braces properly, the model proposed by Uriz et al. [10] is used. In order to trigger global buckling, 0.01% of the brace length is considered as an initial camber at the mid-length of the brace. Corotational transformation is implemented to take into account nonlinear geometry. Local buckling and fracture of the steel brace are not captured by modeling method used in this study. However, the members of the frame meet the slenderness ratio of TBEC [1], thus, it is deemed that frame is able to undergo inelastic deformations before local buckling. A fiber discretization over cross-section is integrated to achieve interaction between axial load and bending moment. Also, five integration points in compliance with the Gauss-Lobatto rule are used along the members. The uniaxial Menegetto-Pinto material [12] (Steel02) is assigned to each fiber elements, which is available in the OpenSees simulation platform.

4.2 Validation of Numerical Model

The modeling techniques used in this study was verified with experimental test results obtained from nonlinear dynamic response of the one-story one-bay IVBF specimen tested by Okazaki et al [19].

Large-scale shake table tests with single-story, single-span, chevron CBF specimen were conducted at E-Defense, Japan by Okazaki et al [19]. A series of strong ground motions were applied to specimen to investigate the dynamic behaviour of steel concentrically braced frame. The CBF specimen has 4.15 m span and 2.25 m height that represent 70% scale of typical building structures as shown Figure 4-1. Materials of the members of specimen are given in Table 2-1. STKR400, SN400, BCR295 and SS440 have minimum yield strength of 245,235,295 and 245 MPa, respectively.

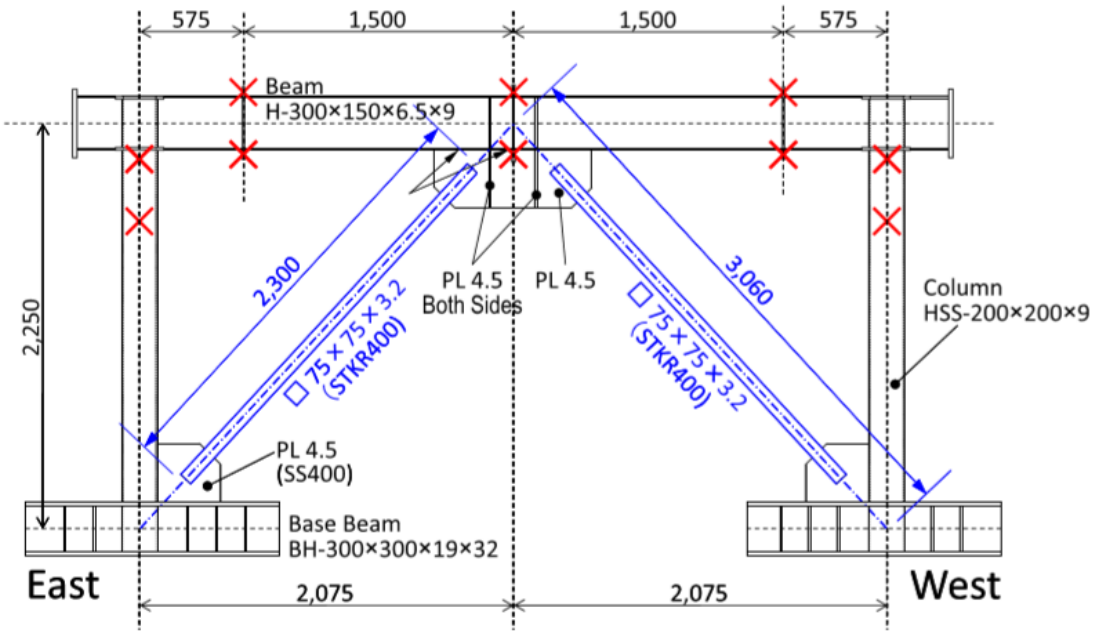

Figure 4-1: Test specimen detail [19]

Table 4-1: Material properties of structural members of test specimen [19].

Material	Designation	F_y (MPa)	F_u (MPa)	Elongation (%)
Brace	STKR400	383	452	36
Beam flange (9 mm)	SN400B	327	456	27
Beam web (6 mm)	SN400B	376	472	29
Column	BCR295	434	518	19
Gusset plate (4.5 mm)	SS400	204	291	54

The east-west (EW) component of the JR Takatori motion which is a strong ground motion record of 1995 Kobe earthquake was applied in the direction parallel to the loading plane. Acceleration history and acceleration spectrum (ζ=0.02) of the motion are given in Figure 4-2 and Figure 4-3, respectively. The shake table tests were carried out seven times. Acceleration response spectra generated with the measured table motion also is shown in Figure 4-3.

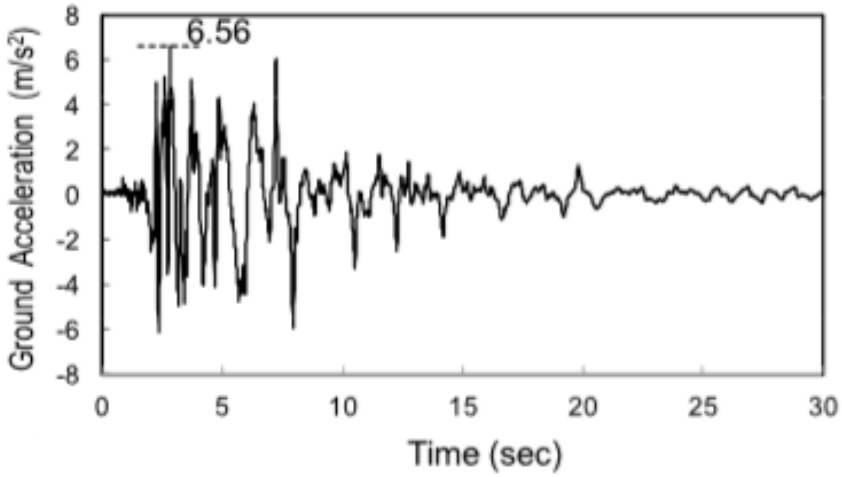

Figure 4-2: JR Takatori acceleration history [19].

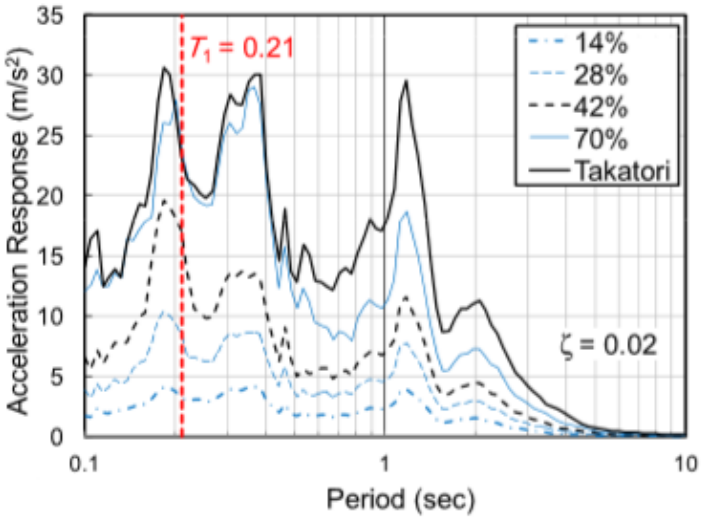

Figure 4-3: Response spectra [19].

Frame results for 28, 42, 70 % motions are given in Figure 2-6 as story shear versus story drift response. It is deduced from the Figure 4-4 that structure behaved linearly under the 28% motion, but nonlinear behaviour occurred during the 48% motion. The frame behaviour under 70% motion drawn in Figure 4-4 (c) shows that system was affected by buckling and yielding of the braces between -0.015 rad and +0.01 rad. When each brace buckled, it brought about a reduction in stiffness and degradation in story shear, though the frame had the ability to win back strength as the drift raised further.

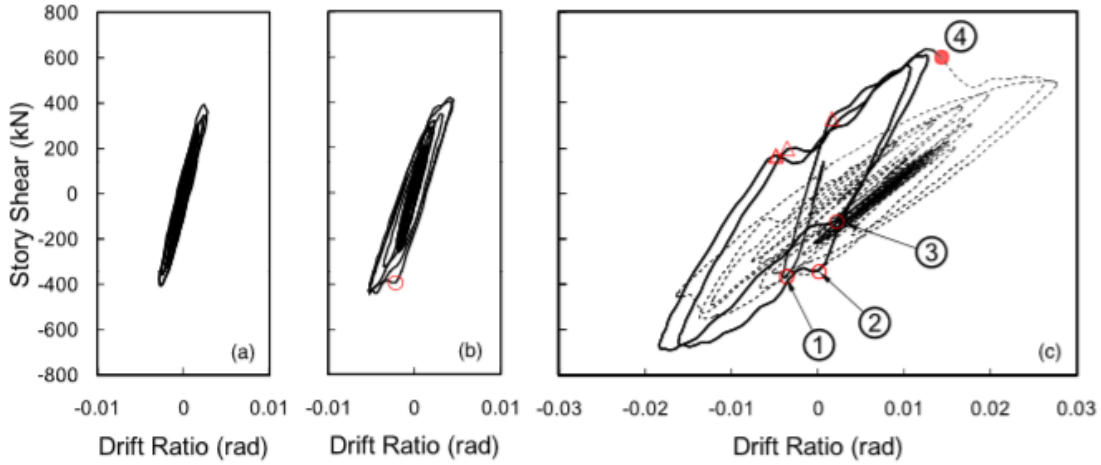

(a) (b) (c)

Figure 4-4 : Frame results from (a) 28, (b) 42 and (c) 70% motion [19]

Figure 4-5 illustrates that axial force-strain relationship of the east brace for the 28, 42 and 70% motion. Also, Figure 2-8 shows the rotation measured from top and bottom ends of the east brace for the aforementioned motions. On the Figure 2-5 and 2-6, P_y and P_{cr} stand for tensile yield strength and compressive strength, respectively. It is concluded that even though the specimen performed similar drifts in compression and tension, the braces experienced larger shortening than elongation. Also, braces did not reach their tensile yield strength.

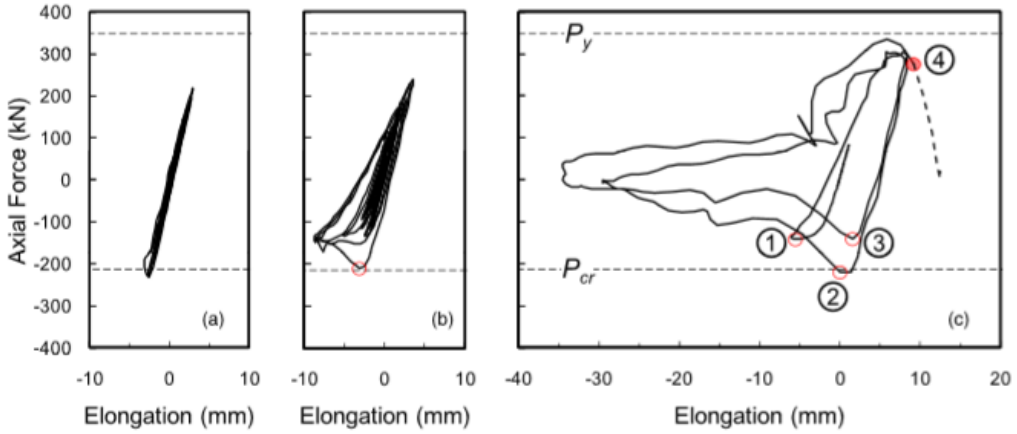

(a) (b) (c)

Figure 4-5: Axial force-strain relationship of east brace from (a) 28, (b) 42 and (c) 70% motion [19].

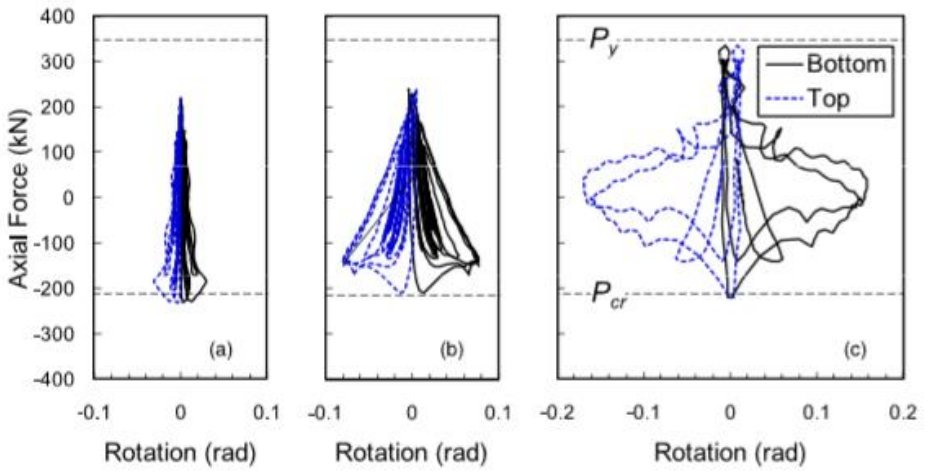

(a) (b) (c)

Figure 4-6: Rotations measured from top and bottom ends of east brace from (a) 28, (b) 42 and (c) 70% motion [19]

Authors concluded that although pushover results obtained from numerical modelling estimate plastic hinge formation at the mid-length of the beam due to unbalanced force, the specimen did not form plastic hinge. Elastic deformation of the beam raised brace shortening and limited brace elongation. Hence, the unbalanced force in the beam was smaller than expected from the pushover results. Figure 4-7 illustrate the pushover results of Okazaki et al. [19] and numerical model of this study on the same plot. From Figure 4-7, plastic hinge forms at the end of the compression brace at 0.01 rad, the brace starts to no longer resist axial force. It can be concluded that numerical model can estimate the plastic hinge formation which is the same as that of Okazaki et al [19].

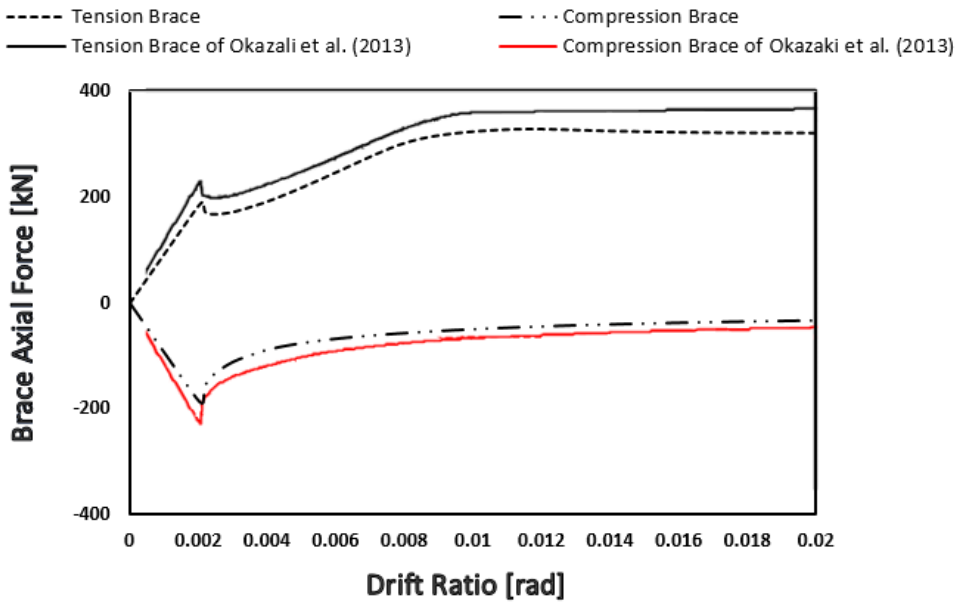

Figure 4-7: Pushover results of experiments by Okazaki et al. [19] and numerical model

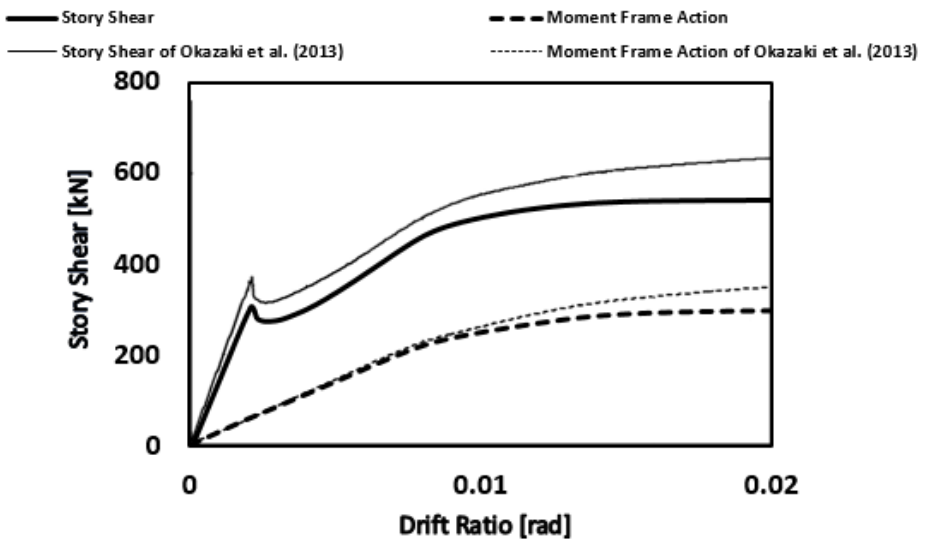

Figure 4-8: Story shear versus drift results of Okazaki et al. [19] and numerical model

For validation of modeling approach of this study, base shear versus drift ratio results of the experiment at the target amplification level of 42% was compared with the analyses results of this study. It can be seen from Figure 4-9 and Figure 4-10 that numerical model of this study is able to capture the overall response. Moreover, numerical model is capable of representing global behavior of the system compared to experimental results. Therefore, it can be stated that numerical model is adequate to simulate the nonlinear performance of CBFs. But the model underestimates the maximum base shear. Maximum base shear is around 415 kN in Okazaki et al. [19] whereas it is approximately 300 kN in the numerical model. Drift ratios that correspond to maximum base shears are approximately 0.0049 and 0.0041 for Okazaki et al. [19] and numerical model, respectively.

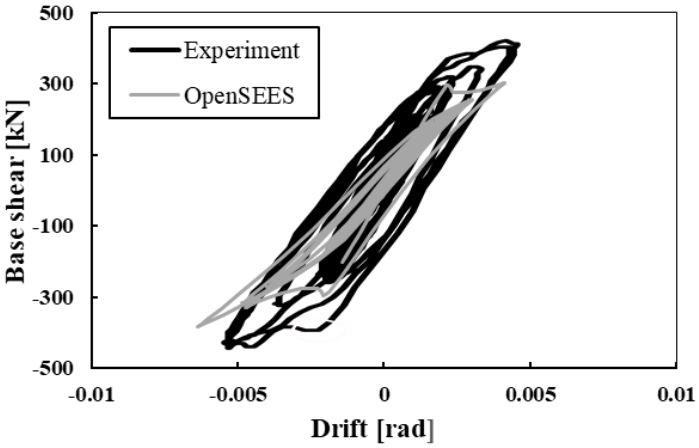

Figure 4-9 : Results of experiments by Okazaki et al. [19] and numerical model

The followings are responsible for the differences between numerical and experimental results,

- Gusset plates were not included in the numerical model. Instead, pin connections were assigned for connecting the brace-to-column and the brace-to-beam. The end zone that includes gusset plates has a larger stiffness when compared to the brace member. Due to excluding gusset plates in the numerical model, the elastic stiffness of the numerical model was less than that of Okazaki [19] by approximately 25%. Therefore, underestimation in base shear force was observed in the numerical model results.
- In the numerical model, the braces were modeled from centerline to centerline. Although the braces in the experiment of Okazaki [19] have total length of 3.06 m. from centerline to centerline, the buckling length of the braces is only 2.3 m. This caused differences between the compressive strength capacity of the numerical model braces and the experimental model braces by 60%. As the larger buckling length decreases the critical buckling stress of brace, braces had less strength compared to experimental model.

CHAPTER V

SEISMIC PERFORMANCE EVALUATION OF STEEL CHEVRON BRACED FRAME PER THE TURKISH BUILDING EARTHQUAKE CODE 2018

As discussed in Chapter 1, TBEC [5] introduces two yield mechanisms and performance levels. To the researchers' knowledge, there is no study in literature evaluating the seismic performance of IVBFs designed per TBEC [5] considering the performance levels in TBEC. In this chapter, a two-story IVBF was designed per TBEC [5] and analyzed under ground motions scaled to the ground motion intensity levels defined in TBEC to evaluate the performance of IVBF per the deformation limits given in TBEC [5].

5.1 Building Design

A two-story office building located in Atasehir, Istanbul was designed in this study per TBEC [5] and TSSC [6]. The floor plan shown in Figure 5-1 was considered in this study. The floor plan is rectangular with side dimensions of 40 m and 30 m. There are four bays in chevron arrangement in the long direction of the floor plan. The braced bays in the short direction of the floor plan were not shown in Figure 5-1 as only the braced bays in the long direction are considered in this study. All beam-to-column connections and the column bases of the IVBF were assumed to be pinned connections. A dead load of 5 kPa and a live load of 2 kPa were considered as the loading. The story height was assumed to be 3 m for both stories. For the design of the frames, the equivalent lateral force method presented in TBEC was conducted. The mapped accelerations for the short period and 1 s period for DD2 ground motion intensity level were extracted from the Turkish Seismic Hazard Maps of AFAD [17] as 0.898 g and 0.248 g, respectively.

The response spectrum was constructed assuming the following parameters: (1) a soil profile of ZB, (2) an importance factor of 1, and (3) a response modification factor of 5. The total seismic weight of the building and the design base shear were calculated as 13440 kN and 1185 kN, respectively. The first two elastic periods in the long direction of the floor plan were 0.458 s and 0.182 s, respectively. The S355JR steel with a nominal yield strength of 355 MPa was used for beams, columns, and braces. Approximate second order analysis prescribed in TSSC was implemented to calculate the required strength of members. The selected sections for the braced bay in the long direction are presented in Table 5-1.

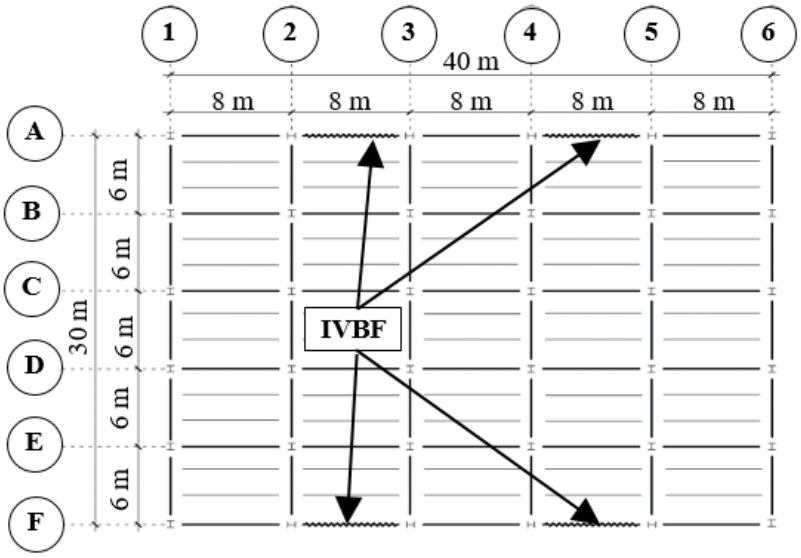

Figure 5-1: Floor plan considered in this study

Table 5-1: Beam, column, and braces sizes of the IVBF.

	Beam	Column	Brace
Story 1	HE550M	HE220A	HSS110x110x8
Story 2	HE500M	HE180A	HSS100x100x8

5.2 Numerical Modeling of Chevron Braced Frame

The seismic performance of the designed building was evaluated by means of numerical analysis. An open-source computational framework, OpenSees [10], was used for numerical simulations. As the building has a regular floor plan, the two-dimensional finite element model of an isolated braced bay in the long direction was deemed to be sufficient to evaluate the seismic performance (Figure 5-2). As there are four braced bays in the long direction, one quarter of the earthquake loads was assumed to act on the isolated braced bay. P-Δ effects were included in the model by adding an axially rigid leaner column with no flexural stiffness. One quarter of the total vertical load of each floor was applied to the leaner column at floor levels. One quarter of the corresponding seismic mass at each story was assigned as lumped masses at beam-column connections. All connections are assumed to be simple connections. To simulate the proper buckling behavior of the braces, the model proposed by Uriz et al [10] was implemented. In this model, a brace member is subdivided into at least two force-based distributed-plasticity nonlinear beam-column elements with an initial imperfection at the common node of these elements. Nonlinear geometry is provided through corotational transformation of nodal displacement between undeformed and deformed geometry. An initial camber of 1/1000 of the braced length was used in this study (Figure 5-1b). Note that the model proposed by Uriz et al. [10] does not consider local buckling and fracture under cyclic loading for brace members. The beams and columns of the frame were modeled using nonlinear beam-column elements as well. The interaction between axial load and bending moment was achieved through the integration of the uniaxial stress-strain relation of fiber over the cross section. The inelastic response was monitored at five sections along the

axis of the members, where these sections were selected in accordance with the integration points of Gauss-Lobatto quadrature rule [20]. The steel material model Steel02 readily available in the OpenSEES library was used for all members. The yield stress was assumed to be 355 MPa (nominal yield strength of S355JR) for the beams and columns while a yield stress of 497 MPa was used for the braces which corresponds to R_yF_y of S355JR. For all materials, a strain hardening ratio of 0.3% was assumed. A Rayleigh damping of 2% was assigned to the first and second modes.

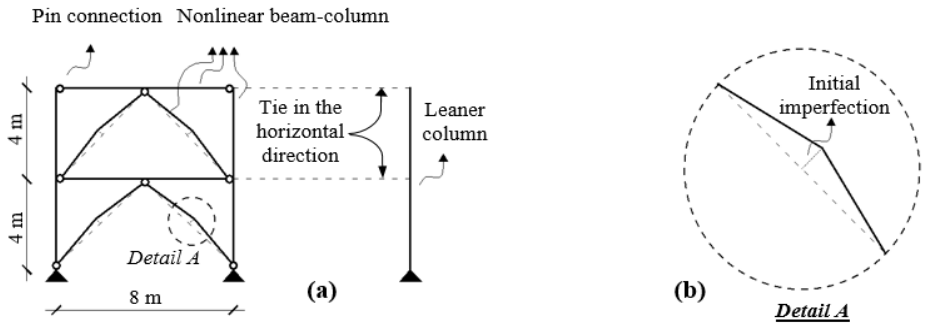

Figure 5-2: 2D model of the IVBF frame: (a) elevation view and (b) initial imperfection.

5.3 Results of Nonlinear Dynamic Analysis

The seismic performance of the IVBF model was assessed per TBEC [5]. Eleven ground ground motions (Table 6-2) were selected from the ground motion database of the Pacific Earthquake Research Center [21] for nonlinear response-history analysis. The selected ground motions were scaled to three ground motion intensity levels, namely, DD1, DD2, and DD3. The ground motions were scaled per TBEC [5] such that the average amplitude of the scaled ground motions was not less than the response spectrum constructed for the target ground motion intensity level between the period values of $0.2T_p$ and 1.5 T_p, where T_p is the fundamental period of the frame. The unscaled response

spectra of the selected ground motions are given in Figure 5-3. In addition, the scale factors for each ground motion under the target intensity level are tabulated in Table 5-2.

Table 5-2: Details of the selected ground motion records.

			Scale Factor		
Earthquake	**Station**	**Year**	**DD1**	**DD2**	**DD3**
Darfield	Heathcote Valley Primary School	2010	1.350	0.730	0.306
Duzce	Lamont 1061	1999	3.327	2.182	0.887
Erzincan	Erzincan	1992	0.603	0.490	0.185
Imperial Valley	Cerro Prieto	1979	1.950	1.262	0.506
Kobe	Takatori	1995	0.416	0.289	0.114
Landers	Coolwater	1992	1.219	0.723	0.304
Landers	Fun Valley	1992	2.738	1.291	0.580
Managua	Managua ESSO	1972	1.644	0.747	0.336
Manjil	Abbar	1990	0.706	0.490	0.190
Parkfield	Cholame Shandon Array #5	1966	2.131	1.014	0.448
Tottori	OKYH14	2000	3.995	2.167	0.853

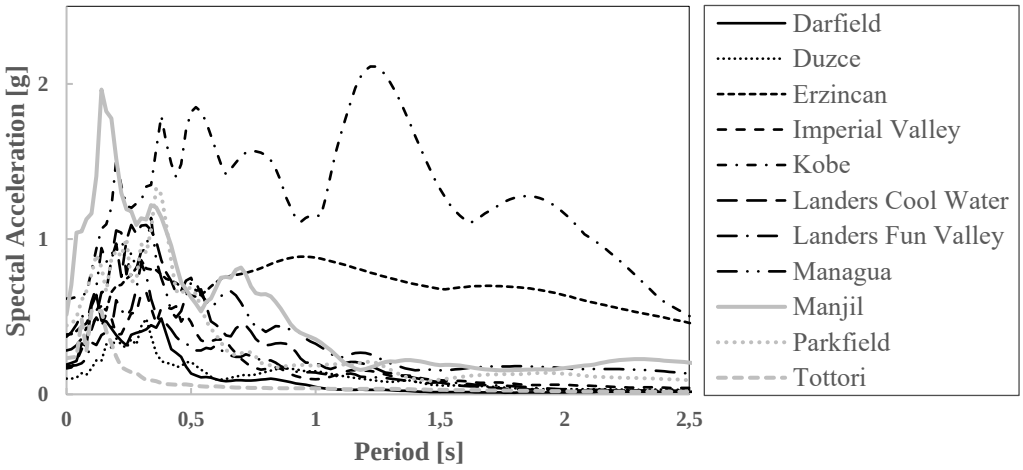

Figure 5-3: 5% damped response spectra for the selected ground motions (unscaled).

The axial deformations at yielding for compression and tension (Δ_C and Δ_T, respectively) are calculated by dividing the expected compressive and tensile strength by the elastic axial stiffness of the brace, respectively. The brace deformation limits defined in TBEC [5] for braces are tabulated in Table 5-3 for three discrete performance levels, namely, SH, KH, and GO.

Table 5-3: Axial plastic deformation limits for HSS braces.

	SH	KH	GO
Compression	0.5 Δ_C	5 Δ_C	7 Δ_C
Tension	0.5 Δ_T	8 Δ_T	11 Δ_T

Figure 5-4 shows the plastic axial shortening and elongation of braces (Δ_p) normalized with respect to the yield displacement, Δ_y, (i.e., either Δ_C or Δ_T) for the first story. As seen in Figure 5-4, the maximum normalized plastic deformation in tension for the first story braces was 5.41 at DD1, which corresponds to the KH performance level. The maximum normalized plastic deformation in compression for the first story braces was 41.1 at DD1, which indicates that the brace failed and led to collapse as the normalized plastic deformation limit in compression for GO is 7 at DD1. TBEC states that the average of the maximum deformations from all eleven nonlinear response-history analyses shall be considered to determine the performance level. The averages of the maximum deformations in tension and in compression for the first story braces at DD1 were 19.2 and 1.0, respectively. Consequently, the first story braces might lead to collapse of the system under compression at DD1. At DD2, the averages of the maximum plastic deformations in compression and in tension were 10.5 and 0.2, respectively. Similar to DD1, the collapse of the system was expected due to the failure of the first story braces in compression at DD2. For DD3, no plastic deformation was observed in tension for the first story braces while the average of the maximum plastic compressive deformations was 3.5 which indicates that the braces exhibited the KH performance.

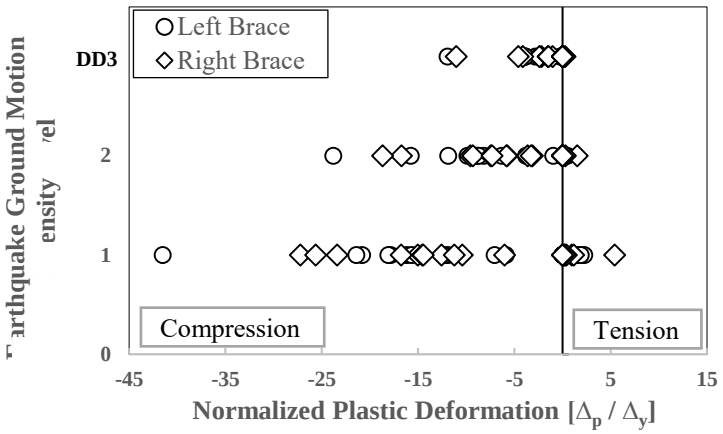

Figure 5-4: Normalized plastic deformation of the first story braces.

Figure 5-5 shows the plastic axial shortening and elongation of braces (Δ_p) normalized with respect to the yield displacement, Δ_y, for the second story. The average normalized plastic deformations in tension and compression were 1.95 and 15.2 at DD1, 0 and 6.5 at DD2, and 0 and 2.2 at DD3, respectively. As a result, the second story braces satisfied the GO and KH performance levels for DD2 and DD3, respectively. At DD1, the second story braces lea to collapse due to failure in compression.

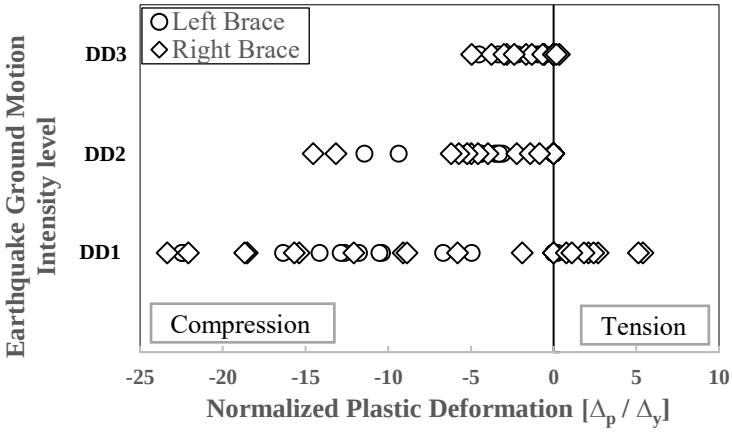

Figure 5-5: Normalized plastic deformation of the second story braces.

Figure 5-6 displays the beam rotations at the midspan (θ) normalized with respect to the yield rotation (θ_y). The plastic hinge length at the midspan of the beam was assumed to be equal to the one-third of the beam length per TBEC [5]. Please note that this plastic hinge length given in TBEC is for the plastic hinges at the end of the beams that undergo double curvature; however, it was deemed appropriate to assume the same length for the plastic hinge the beams of IVBFs as they are simply supported beams with a concentrated load at the midspan (that is the vertical component of the resultant of the brace forces). The rotations at DD1, DD2, and DD3 for both story beams were well below θ_y, i.e., the beams remain elastic, which can be attributed to the fact that the beams are capacity-designed to remain elastic. Consequently, it can be inferred that the beams exhibit desirable performance. Satisfied performance levels for braces are tabulated in Table 5-4.

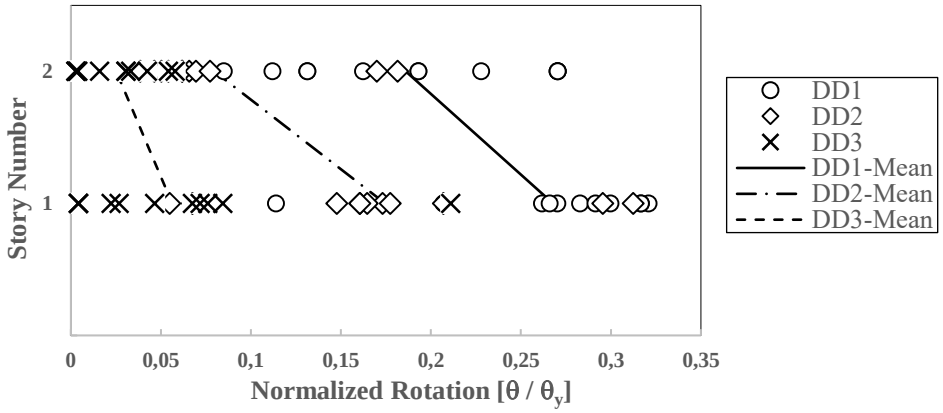

Figure 5-6: Normalized beam rotations at the midspan

Table 5-3: Satisfied performance levels for the first and second story braces

	DD-1		DD-2		DD-3	
	T	C	T	C	T	C
First Story	KH (RIGHT BRACE)	COLLAPSE (LEFT BRACE)	SH (RIGHT BRACE)	COLLAPSE (LEFT BRACE)	---	KH (LEFT BRACE)
Second Story	KH (RIGHT BRACE)	COLLAPSE (RIGHT BRACE)	---	GO (RIGHT BRACE)	---	KH (RIGHT BRACE)

T = Tension, C = Compression

Figure 5-7 depicts the column plastic rotations (θ_p) normalized with respect to the yield rotations (θ_y). It is worthwhile noting that the beam-column connections and the column bases were assumed to be simple connections; therefore, the columns were expected to resist no moment. However, due to the contiunity of the columns along the building height, flexural demands appeared to develop in columns when there was differential drift between adjacent stories which caused column rotations at floor levels (Figure 5-7). As seen in Figure 5-7, these flexural demands associated with differential drifts (Figure 5-8) led to plastic rotations in the columns of IVBFs at floor levels (at the first floor level for the IVBF considered in this study). Even if the plastic rotations observed in the column of this particular study were very small and might be negligle, they may be critical for IVBFs that can exhibit significant differential drifts between adjacent stories.

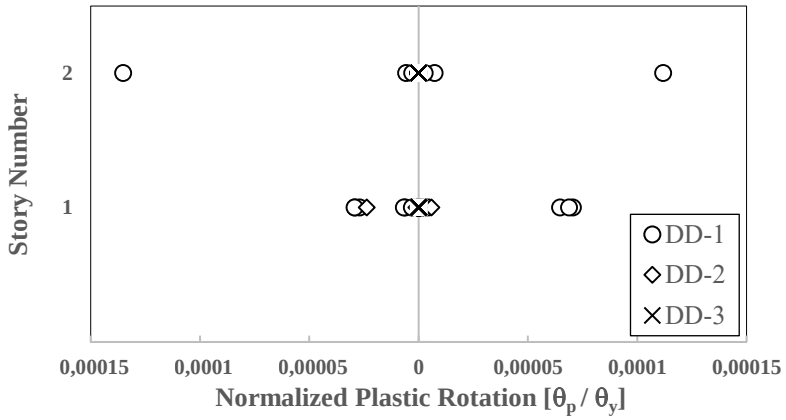

Figure 5-7: Normalized column plastic rotations

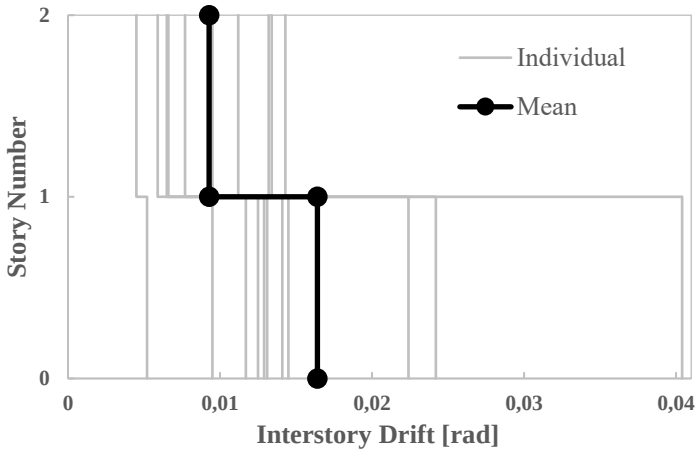

Figure 5-8: Interstory Drift at DD1

CHAPTER VI

COLLAPSE ASSESSMENT OF STEEL CHEVRON BRACE FRAME BY USING INCREMENTAL DYNAMIC ANALYSIS

It is needed that seismic capacity of CBFs should be reliably identified in order to predict the global instabilities of CBFs that undergoes inelastic response when it is subjected to severe earthquakes. For this purpose, many approaches have been proposed by several researchers as well as the guidelines (e.g. FEMA P-695). Incremental Dynamic Analysis (IDA), one of the proposed approaches, was propounded by Bertero [22] at first, which was applied to structures to trace the dynamic behaviour of them through collapse. Then, Vamvatsikos and Cornell [23] introduced a new concept and definitions for IDA approach. IDA is a parametric analysis method to evaluate seismic performance of structures extensively under a number of ground motion records. Nonlinear dynamic analyses are conducted with increasing intensity levels repeatedly. Results obtained from nonlinear dynamic analyses are plotted on the same plot, which forms IDA curve in which vertical axis indicates Intensity Measure (IM) and horizontal axis indicates Damage Measure (DM) or Engineering Demand Parameter (EDP) as shown on sample IDA curve in Figure 6-1.

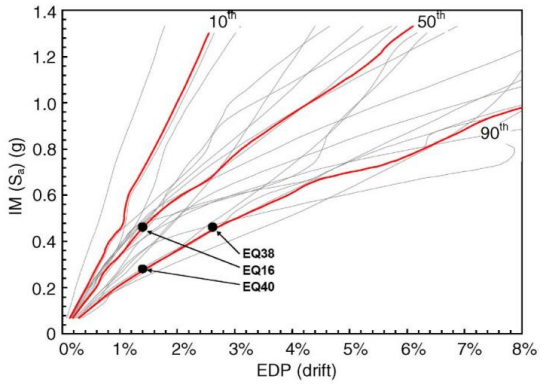

Figure 6-1: Incremental dynamic analysis curves (adapted from Rodgers et al. 2012)

This chapter gives incremental dynamic analyses results of 2-story CBF designed to newly introduced TBEC [5]. To the best of the author's knowledge, there is no study that examines the collapse performance of CBFs designed per TBEC. For this purpose, eleven ground motions were applied to 2-story CBF with incrementally spectral acceleration and then IDA curves were drawn.

6.1 Building Design

The structure, two-story building located in Atasehir, Istanbul, was developed by utilizing the rules of TBEC [5] and TSSS [6] . The building has rectangular floor plan with 30 m and 40 m dimensions for long and short direction, respectively. Connections of beam-to-column and brace-to-beam were assigned as pinned connections. Lateral load resistance of building was provided by four chevron type braced bay in each floor of building in the long direction.

A dead load of 5 kPa and a live load of 2 kPa were assigned to building. To calculate the required strength of members, tributary area method was employed, and equivalent earthquake load method proposed by TBEC [5] was implemented. Since DD-2 earthquake ground motion intensity level is considered by TBEC [5] as design basis earthquake level for calculation of earthquake loads, the mapped accelerations for the short period and 1 s period were obtained from the Turkish Seismic Hazard Maps of AFAD [17] as 0.898 g and 0.248 g, respectively, for DD-2 intensity level that characterize the earthquake ground motion with a 10% probability of exceedance in 50 years. The target response spectrum was generated with the using following parameters that depend on construction area and building type: (1) a soil profile of ZB (medium hard rock soil), (2) an importance factor of 1, and (3) a response modification factor of 5 owing to high-ductility level building. The total seismic weight of the building and the design base shear

were calculated as 13440 kN and 1185 kN, respectively. The first two elastic periods in the long direction of the floor plan were 0.451 s and 0.179 s, respectively. The S355JR steel with a nominal yield strength of 355 MPa was used for beams, columns, and braces. Approximate second order analysis prescribed in TSSC [6] was implemented to calculate the required strength of members. The selected section for the braced bay in the long direction are shown in Figure 6-2.

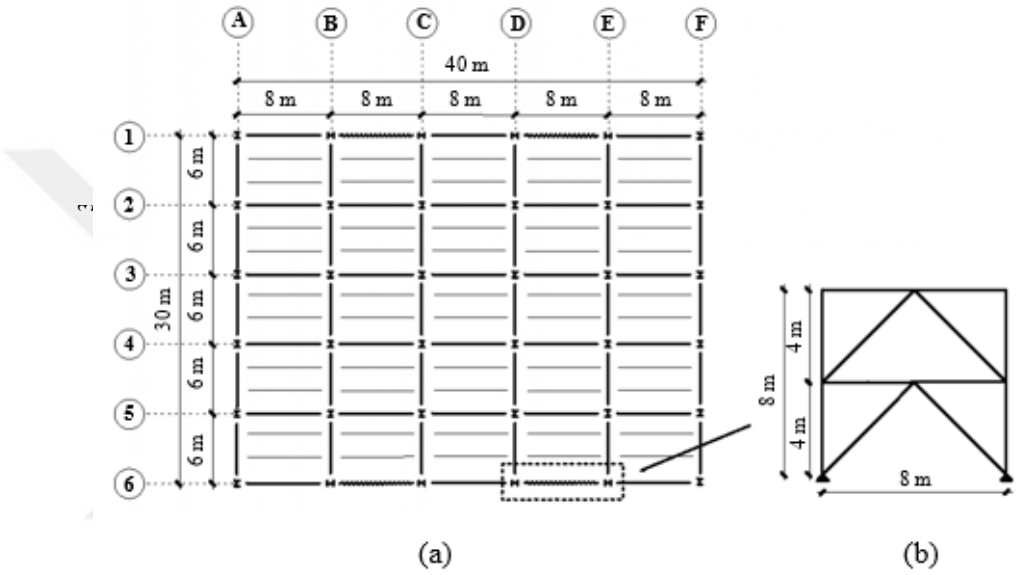

Figure 6-2: (a) Plan view of building and (b) elevation view of braced bay used in this study

6.2 Numerical Modeling of Chevron Braced Frame

The nonlinear dynamic analyses of structural model were carried out in OpenSees simulation platform [18]. The two-dimensional finite element model (Figure 6-3) of a one braced bay in the long direction was found to be reasonable for nonlinear dynamic analysis since the building has a regular floor plan. A leaner column was used to include P-Δ effects of the gravity load resisting part of the building. One fourth of the total vertical load of each floor was applied to the leaner column at floor levels. One quarter of the corresponding seismic mass at each story was assigned as lumped masses at beam-column

connections. To simulate the post-buckling behavior of the steel braces, the model proposed by Uriz et al. [10] was employed. The brace member was divided into two force-based distributed-plasticity nonlinear beam-column elements with an initial imperfection that is assumed to trigger global buckling. Nonlinear geometry was taken into account through corotational transformation of nodal displacement between undeformed and deformed geometry. A 0.01% of the brace length was used for initial camber (Figure 6-4a). It should be highlighted that local buckling and fracture of steel brace are not captured by the modeling approach used herein. Moreover, since the members of the frame meet the slenderness ratio limits of TBEC [5], it is assumed to be able to undergo considerable inelastic deformations prior to onset of local buckling. A fiber-based approach (Figure 6-4b) was utilized to generate cross sections of beams, columns and braces in order to account for the interaction between axial load and bending moment. As suggested by Coleman and Spacone [24], odd-numbered integration points, five integration points, were used along the axis of the members in compliance with the Gauss-Lobatto quadrature rule [20] to capture the lateral displacement of the mid-length of the braces. In addition, five integration points provide proper spreading and integration of inelastic curvature along the brace to avoid sudden stiffness change in the brace [25]. The uniaxial Menegetto-Pinto material [12] (Steel02) was assigned to each fiber elements, which is available in the OpenSees simulation platform (Figure 6-4c). The yield stress of beams and columns was assumed to be 355 MPa (nominal yield strength of S355JR) while a yield stress of 497 MPa was used for the braces which corresponds to R_yF_y of S355JR. For all materials, a strain hardening ratio (b) of 0.3% was assumed. A Rayleigh damping of 2% was assigned to the first and second modes.

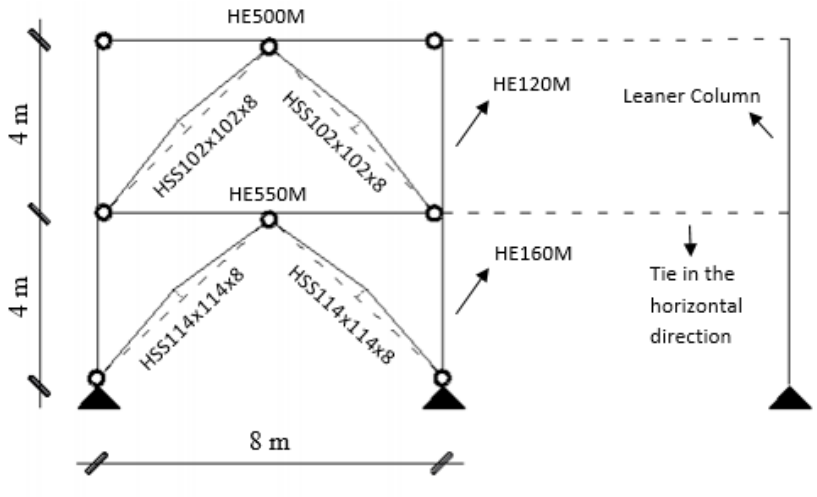

Figure 6-3: (a) 2D model of CBF constructed in OpenSees and section details

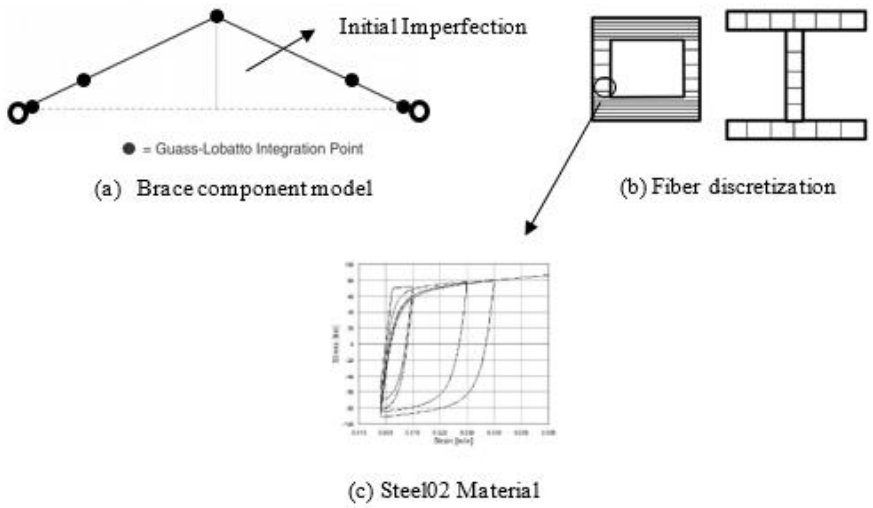

Figure 6-4: (a) Brace component model, (b) fiber discretization and (c) Steel02 material

6.3 Results of Nonlinear Dynamic Analysis

Incremental Dynamic Analysis (IDA) was employed to identify the collapse capacity of 2-story IVBF, which applies repetitive nonlinear dynamic analysis to the frame by scaling the amplitude of a set of ground motions. With the results of several ground motions, increasing intensity levels versus response of structure were drawn on the same plot for each ground motions, which forms the IDA Curve Set. In IDA curve,

while the Intensity Measure signifies the intensity of ground motion, Damage Measure (DM) characterize the response of the structure subjected to the several ground motions. Although there are several possible choices to represent the IM and DM, the 5% damped spectral acceleration at the first mode period of the structure $S_a\ (T_1, 5\%)$ and the maximum interstory drift ratio (θ_{max}) are commonly used for IM and DM,respectively.For nonlinear response-history analysis, eleven ground ground motions were selected from the Pacific Earthquake Research Center (PEER) ground motion database [21]. The selected ground motions were scaled to DD-1 ground motion intensity level at the fundemental period of the frame (T_p) that was 0.45 s. The unscaled response spectra of the selected ground motions are given in Figure 6-5. In addition, the details of selected ground motions tabulated in Table 6-1.

Table 6-1: Details of the Selected Ground Motion Records

Earthquake	Station	Year
Darfield	Heathcote Valley Primary School	2010
Duzce	Lamont 1061	1999
Erzincan	Erzincan	1992
Imperial	Cerro Prieto	1979
Kobe	Takatori	1995
Landers	Coolwater	1992
Landers	Fun Valley	1992
Managua	Managua ESSO	1972
Manjil	Abbar	1990
Parkfield	Cholame Shandon Array #5	1966
Tottori	OKYH14	2000

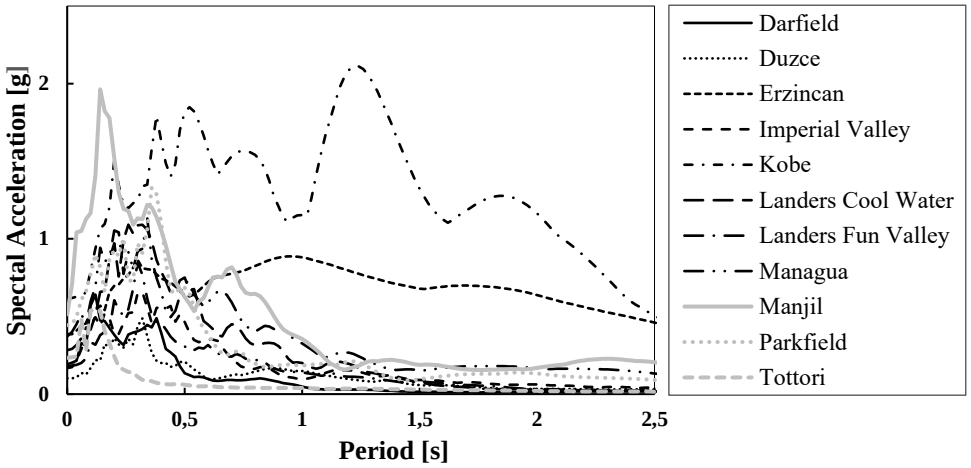

Figure 6-5: 5% damped response spectra for the selected ground motions (unscaled).

6.4 Collapse Limit States

For defining the capacity point of IDA curve, two criteria were introduced, namely IM-based rule and DM-based rule [23]. IM-based rule divides the IDA curve into two regions as non-collapse and collapse region. The point that has tangent slope equal to 20% of elastic slope where the curve reaches a plateau indicating the instability is stated by FEMA/SAC guidelines 350 and 351 [26,27] for IM-based rule. DM-based rule defines that if the drift ratio exceeds the $\theta = 0.1$, collapse limit is achieved. It should be noted that 0.1 drift ratio limit is not convenient for CBFs. For this reason, collapse might occur at less than 0.1 drift ratio in CBFs. When one of the two rules is obtained, it is considered as a capacity point, thus IM-based rule determine the imminent collapse, while DM-based rule guard against extreme values of drift ratio.

The IDA curve draws a proportional part up to certain value where the slope of this part (ratio of IM to DM) is called elastic stiffness (K_e) of given IDA curve. After this elastic range, curve can perform abrupt softening with large drifts and move towards the collapse (Figure 6-6b). Besides, curve can traipse about the slope of elastic range (Figure

6-6a), which is called hardening behaviour, and it reaches a softening curve finally as DM rises at increasingly higher rate, which indicates the onset of dynamic instability.

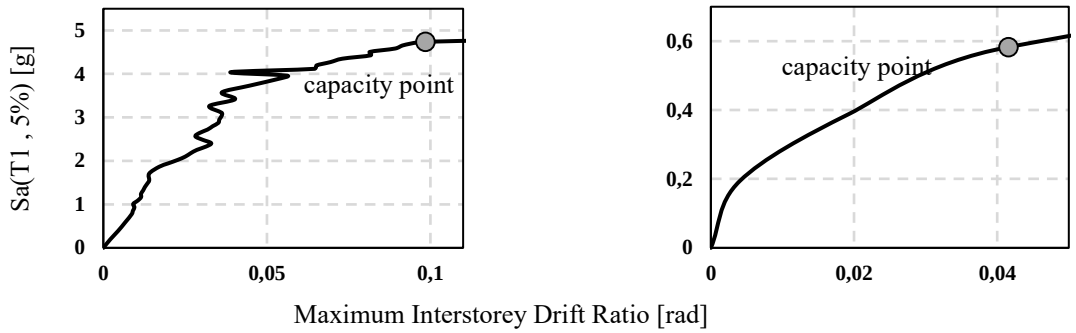

(a) Weaving behaviour (b) Sharply softening behaviour

Figure 6-6: IDA curves of the CBF subjected to the (a) Imperial Earthquake ground motions record and (b) Kobe Earthquake ground motions record

Because of hardening issue, more than one points may satisfy the limit state. In this case, the last point on the curve with a slope equal to 20% of elastic slope is determined as a capacity point. As shown in Figure 6-7a, point B was selected as a capacity point rather than point A which satisfy the IM-based rule firstly. This phenomenon is referred to as structural resurrection. Furthermore, extreme resurrection phenomenon (Figure 6-7b) where the system is pushed to the global collapse under a certain IM, only to reappear as non-collapsing at a higher intensity level, performing high response but still standing [23].

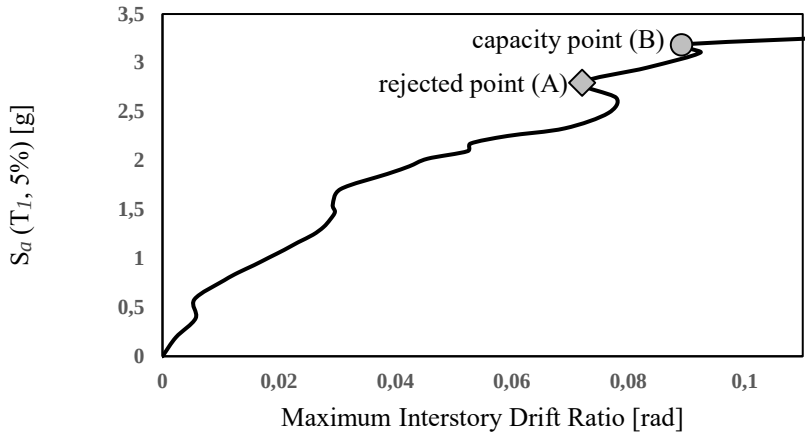

(a) IDA curve of Tottori ground motion

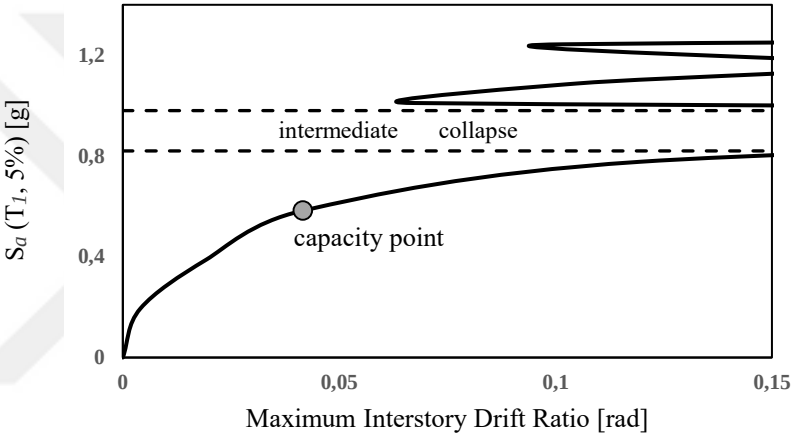

(b) IDA curve of Kobe ground motion

Figure 6-7: (a) Resurrection phenomenon; (b) extreme resurrection phenomenon

Figure 6-8 shows the IDA curves of the CBF considered in this study under eleven ground motions in terms of 5% damped spectral acceleration versus maximum interstory drift ratio. Capacity points that marked with dotted point on the IDA curves were determined by using FEMA/SAC [26, 27] guidelines.

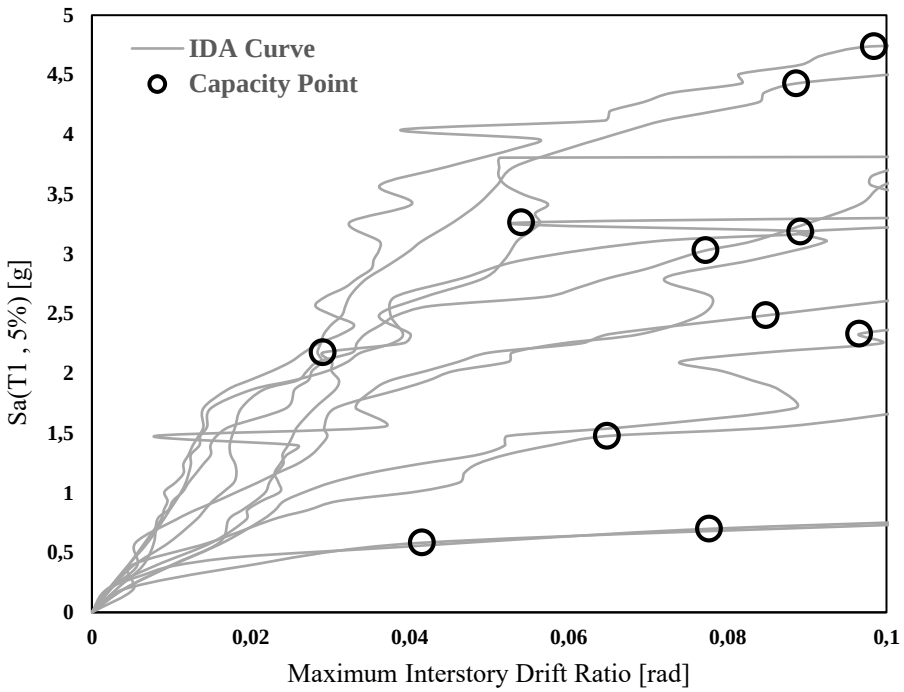

Figure 6-8: IDA curves for eleven ground motions and capacity points defined according to FEMA/SAC guidelines.

Collapse level ground motions are defined as intensity that would cause median collapse of structures by FEMA P-695 [28]. When one-half of the structures used in analyses are exposed to these collapse level ground motions, median collapse is considered to be taken place. As defined in FEMA P-695 [28], collapse margin ratio (CMR) is ratio of median spectral acceleration of the collapse level ground motions $(\hat{S}_{CT})$ to spectral acceleration of the maximum considered earthquake (MCE) ground motion (S_{MT}).

Using the collapse data extracted from IDA results, the collapse fragility curve (Figure 6-9) was constructed by means of FEMA P-58 Conditional Probability of Collapse Curve Fit Tool [29]. The median collapse level $(\hat{S}_{CT})$ was calculated as 2.15 g while Maximum Considered Earthquake ground motion demand (S_{MT}) was 0.772 g. The collapse margin ratio therefore was 2.78.

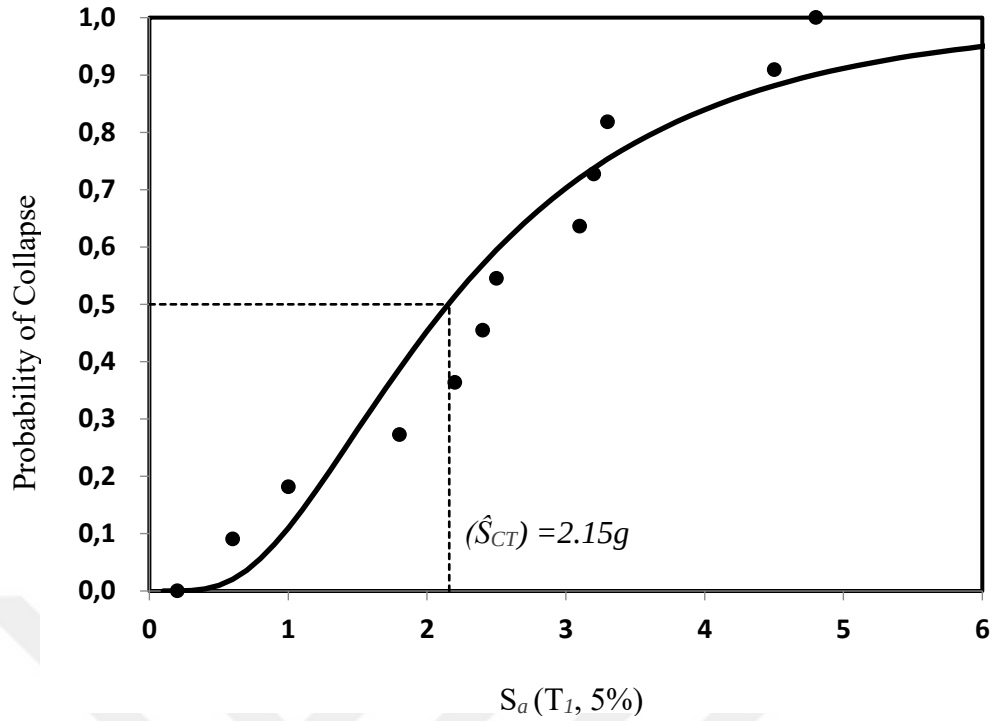

Figure 6-9: Collapse fragility curve of the chevron braced frame

6.5 Acceptability of Collapse Margin Ratio

Determination of collapse margin ratio (CMR) can be significantly affected by the spectral shape of selected ground motions. In order to take the effects of spectral shape on collapse margin ratio into account, it is adjusted to get the adjusted collapse margin ratio (ACMR) as defined in FEMA P-695 [28] (Equation 6-1).

$$ACMR = SSF \; x \; CMR \tag{6-1}$$

Spectral shape factors are selected from Table 7-1a and Table 7-1b of FEMA P-695 [28] based on fundamental period of the structure (T) and period-based ductility (μ_T) for the corresponding seismic design category (SDC). Period-based ductility is defined in FEMA P-695 [28] as follows (Figure 6-10);

$$\mu_T = \frac{\delta_u}{\delta_{y,eff}} \tag{6-2}$$

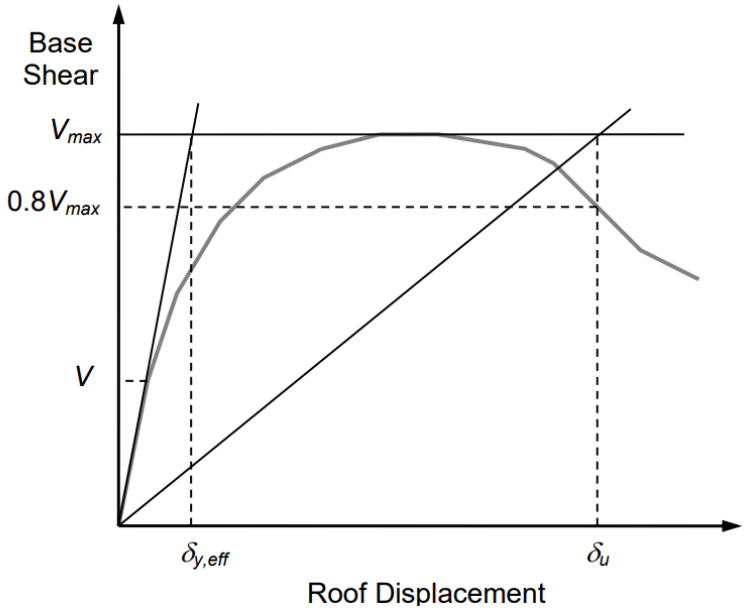

Figure 6-10: Idealized nonlinear static pushover curve (adopted from FEMA P-695)

In Figure 6-10, V_{max} represents the maximum base shear force on the pushover curve and δ_u stands for the ultimate displacement that corresponds to V_{max}. Also, $\delta_{y,eff}$ represents the effective yield displacement.

In order to consider the non-simulated collapse modes when evaluating ultimate roof drift (δ_u), ultimate drifts at non-simulated collapse for the first story and second story were defined in Figure 6-11 and Figure 6-12, respectively. For the second story, it is assumed that collapse occurs at 0.1 drift ratio. It was found that first non-simulated collapse occurs at 174. step of the pushover analysis at first story. Drift ratio that corresponds to 174. step of the pushover analysis for the roof drift displacement was marked on roof drift versus base shear force curve (Figure 6-13) and it was stated as ultimate roof drift ratio.

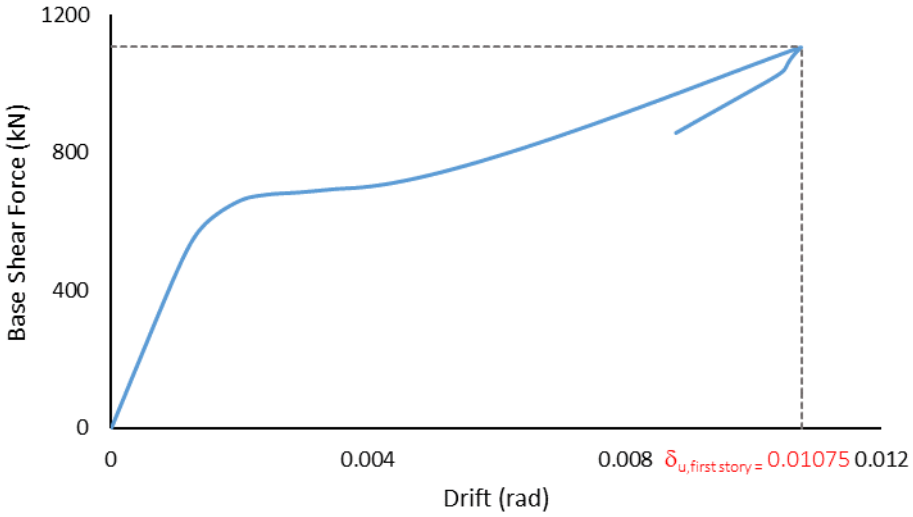

Figure 6-11: Pushover curve for the first story of the building

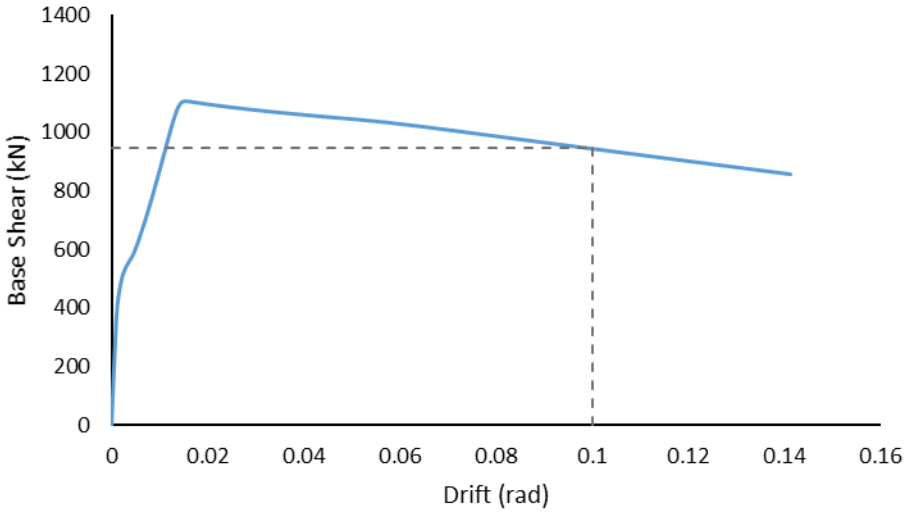

Figure 6-12: Pushover curve for the second story of the building

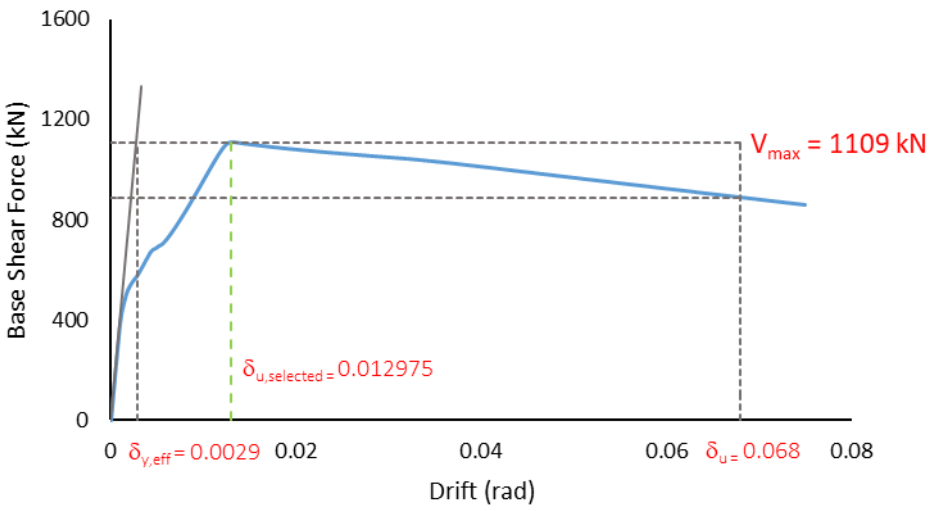

Figure 6-13: Roof drift versus base shear force curve

Period-based ductility (μ_T) of the building was calculated as 4.47 (0.012975/0.0029) from the nonlinear static pushover curve obtained by pushover analysis conducted on the building.

SSF was determined as 1.1041 by interpolating from Table 6-2 considering that fundamental period of the building is 0.45 sec. and μ_T is 4.47 as calculated above for SDC D_{min}. Therefore, ACMR is calculated as 3.07.

Table 6-2: Spectral shape factors (adopted from Table 6-2 of FEMA P-695)

T (sec.)	Period-Based Ductility, μ_T							
	1.0	1.1	1.5	2	3	4	6	≥ 8
≤ 0.5	1.00	1.02	1.04	1.06	1.08	1.09	1.12	1.14
0.6	1.00	1.02	1.05	1.07	1.09	1.11	1.13	1.16
0.7	1.00	1.03	1.06	1.08	1.10	1.12	1.15	1.18
0.8	1.00	1.03	1.06	1.08	1.11	1.14	1.17	1.20
0.9	1.00	1.03	1.07	1.09	1.13	1.15	1.19	1.22
1.0	1.00	1.04	1.08	1.10	1.14	1.17	1.21	1.25
1.1	1.00	1.04	1.08	1.11	1.15	1.18	1.23	1.27
1.2	1.00	1.04	1.09	1.12	1.17	1.20	1.25	1.30
1.3	1.00	1.05	1.10	1.13	1.18	1.22	1.27	1.32
1.4	1.00	1.05	1.10	1.14	1.19	1.23	1.30	1.35
≥ 1.5	1.00	1.05	1.11	1.15	1.21	1.25	1.32	1.37

Acceptable values of ACMR are defined in FEMA P-695 [28] based on total system uncertainty and acceptable probability of collapse. FEMA P-695 [28] suggests that probability of collapse due to Maximum Considered Earthquake ground motions (MCE) should be limited to 10% ($ACMR_{10\%}$). Many sources of uncertainty can affect the collapse capacity. For this reason, it is important to incorparate the all sources of uncertainty in the collapse assessment of the building. Total system collapse uncertainty (β_{TOT}) is defined in FEMA P-695 [28] as follows;

$$\beta_{TOT} = \sqrt{\beta_{RTR}^2 + \beta_{DR}^2 + \beta_{TD}^2 + \beta_{MDL}^2} \tag{6-3}$$

β_{RTR} = record-to-record uncertainty

β_{DR} = design requirements-related collapse uncertainty

β_{TD} = test data-related collapse uncertainty

β_{MDL} = modeling-related collapse uncertainty

For the performance evaluation, since there are wide range of experimental study on behavior of the CBFs and design requirements of the CBFs well established, β_{DR} and β_{TD} were selected as 0.10 from Table 3.1 and Table 3.2 of FEMA P-695 [28], respectively. Also, β_{MDL} was selected as 0.35 from Table 5.3 of FEMA P-695 [28].

Since the μ_T is bigger than 3, β_{TOT} was selected as 0.550 considering that model quality is C (fair) from the Table 6-3.

Table 6-3 : Total system collapse uncertainty (β_{TOT}) for Model Quality (C) Fair and period-based ductility, $\mu_T \geq 3$ (adopted from Table 7-2c of FEMA P-695)

Quality of Test Data	Quality of Design Requirements			
	(A) Superior	(B) Good	(C) Fair	(D) Poor
(A) Superior	0.550	0.575	0.650	0.725
(B) Good	0.575	0.600	0.675	0.750
(C) Fair	0.650	0.675	0.725	0.800
(D) Poor	0.725	0.750	0.800	0.875

Acceptable ACMR values are presented in Table 6-4 for four different collapse probability based on total system uncertainty. For the 10% collapse probability that is suggested by FEMA P-695 [28] Methodology, acceptable ACMR was selected as 2.02. CMR can defined as a ratio that reflects the margin to be reached the collapse of the building by 50% of the ground motions. Since the margin ratio of the building is bigger than acceptable ratio given by FEMA P-695 [28], ACMR ratio passes the $ACMR_{10\%}$ criteria of FEMA P-695.

Table 6-4: Acceptable values of ACMR (adopted from Table 7-3 of FEMA P-695)

Total System Collapse Uncertainty	Collapse Probability				
	5%	10% ($ACMR_{10\%}$)	15%	20% ($ACMR_{20\%}$)	25%
0.275	1.57	**1.42**	1.33	**1.26**	1.20
0.300	1.64	**1.47**	1.36	**1.29**	1.22
0.325	1.71	**1.52**	1.40	**1.31**	1.25
0.350	1.78	**1.57**	1.44	**1.34**	1.27
0.375	1.85	**1.62**	1.48	**1.37**	1.29
0.400	1.93	**1.67**	1.51	**1.40**	1.31
0.425	2.01	**1.72**	1.55	**1.43**	1.33
0.450	2.10	**1.78**	1.59	**1.46**	1.35
0.475	2.18	**1.84**	1.64	**1.49**	1.38
0.500	2.28	**1.90**	1.68	**1.52**	1.40
0.525	2.37	**1.96**	1.72	**1.56**	1.42
0.550	2.47	**2.02**	1.77	**1.59**	1.45
0.575	2.57	**2.09**	1.81	**1.62**	1.47
0.600	2.68	**2.16**	1.86	**1.66**	1.50
0.625	2.80	**2.23**	1.91	**1.69**	1.52
0.650	2.91	**2.30**	1.96	**1.73**	1.55
0.675	3.04	**2.38**	2.01	**1.76**	1.58
0.700	3.16	**2.45**	2.07	**1.80**	1.60
0.725	3.30	**2.53**	2.12	**1.84**	1.63
0.750	3.43	**2.61**	2.18	**1.88**	1.66
0.775	3.58	**2.70**	2.23	**1.92**	1.69
0.800	3.73	**2.79**	2.29	**1.96**	1.72
0.825	3.88	**2.88**	2.35	**2.00**	1.74
0.850	4.05	**2.97**	2.41	**2.04**	1.77
0.875	4.22	**3.07**	2.48	**2.09**	1.80
0.900	4.39	**3.17**	2.54	**2.13**	1.83
0.925	4.58	**3.27**	2.61	**2.18**	1.87
0.950	4.77	**3.38**	2.68	**2.22**	1.90

CHAPTER VII

CONCLUSION

7.1 Conclusions

The two story IVBFs was designed according to implications of TBEC [5] and TSSS [9]. Two different nonlinear time-history analyses were conducted on IVBFs. In the first analyses phase, the numerical model constructed in OpenSees [18] was analysed at three ground motion intensity levels defined in TBEC [5]. The seismic performance of the IVBF was assessed considering the deformation levels given for braces and performance levels of the IVBF which is based on plastic deformations. As a result, under the selected and scaled ground motions for this study, the beams remained essentially elastic at all three ground motion intensity levels. But the columns underwent plastic rotations that were not assumed at the design stage.The plastic deformation demands in the first story braces exceeded the deformation limit given for the collapse prevention at DD1 and DD2. At DD3, the first-story braces satisfied the criterion for the KH performance level. The second-story braces might lead to collapse at DD1 while they exhibited the GO and KH performance at DD2 and DD3, respectively.

In the second analyses phase, incremental dynamic analyses (IDA) [23] were conducted on chevron braced frame. Capacity points were determined on IDA curves extracted from analyses. Finally, collapse fragility curve was developed and collapse margin ratio was calculated. In order to evaluate the acceptability of CMR, ACMR was calculated. Then, acceptable value of ACMR was determined by incorporating the sources of uncertainty. Finally calculated ACMR of the system is bigger than ACMR limit defined by FEMA P-695 [28], this value is accepted.

7.2 Future Works

Numerical model can be improved by adding gusset plates instead of pinned connections. With the improved numerical model, several structures in different configurations might be examined by conducting IDA per FEMA P-695 [28].

BIBLIOGRAPHY

[1] FEMA-355E, "State of the Art Report on Past Performance of Steel Moment-Frame Buildings in Earthquakes," *FEMA*-355E, Washington, DC, 2000.

[2] Bubela, R.K. (2003) "An Experimental and Analytical Study of Chevron Braced Frames with Vertical Slotted Connections" M.S. thesis, University of British Columbia, Vancouver, Canada.

[3] Shibata,M., and Wakabayshi, M. (1983). "Experimental study on the hysteretic behaivour of K-type braced frame subjected to repeated load." Trans. Arch. Inst. Jap., 326,10-16

[4] Fukuta,T., Nishiyama, I. Yamanouchi,H.,and Kato B, (1989)."Seismic performance of steel frames with inverted V braces." J. Struct. Eng., 115(8), 2016-2018.

[5] TBEC. Turkey Disaster and Emergency Management Authority, "Turkish Building Earthquake Code", Ankara,Turkey,2018

[6] Ministry of Environment and Urban Planning, "Turkish Specification of Steel Structures," Ankara,Turkey, 2016.

[7] TEC. (2007) Turkish Earthquake Code, Ministry of Public Works and Settlement, Ankara, Turkey, 2018.

[8] Sen, Andrew D., Roeder, Charles W., Berman, Jeffrey W., Lehman, Dawn E., Li, Chao-Hsien, Wu, An-Chien, and Tsai, Keh-Chyuan. (2016). "Experimental Investigation of Chevron Concentrically Braced Frames with Yielding Beams". J. Struct. Eng., 04016123.

[9] Terpstra, Clare (2017) "Impact of Beam Strength on Seismic Performance of Chevron Concentrically Braced Frames." M.S. thesis, University of Washington, Seattle.

[10] P. Uriz, "Towards earthquake resistant design of concentrically braced steel structures," 2005.

[11] R. G. Black et al., Inelastic Buckling of Steel Struts Under Cyclic Load Reversals. Berkeley, Calif.; Springfield, Va.: Earthquake Engineering Research Center, University of California ; For sale by the National Technical Information Service, U.S. Dept. of Commerce, 1980.

[12] B. V. V. Filippou F.C., Popov E.P., "Effects of Bond Deterioration on Hysteretic Behaviour of Reinforced Concrete Joints," Earthquake Engineering Research Center. pp. 1–212, 1983.

[13] Lee, S., and Goel, S.c. (1987). "Seismic behavior of hollow and concrete filled square tubular bracing members." UMCE87-11, College of Engineering, Univ.of Michigan, Ann Arbor, Mich.

[14] Hsiao, P-C, Lehman, D.E., Roeder, C.W. (2013a). A model to simulate special concentrically braced frames beyond brace fracture. Earthquake Engineering and Structural Dynamics, 42: 183-200.

[15] Khatib, I.F., and Mahin, S.A.1987. Methods for Improving the Seismic Response of Concentrically Braced Steel Frames, In Dynamics of Structures, edited by J.M. Roesset, ASCE, New York, New York, pp. 101-116.

[16] Remennikov, A.M., and Walpole, W.R 1998. Seismic Behaviour and Deterministic Design Procedures for Steel V-Braced Frames. Earthquake Spectra, 14(2): 335-355.

[17] Turkey Disaster and Emergency Management Authority, “Turkish Seismic Hazard Maps,” 2018. [Online]. Available: https://tdth.afad.gov.tr/. [Accessed: 20-Aug-2019].

[18] McKenna, F. T. (1997). Object-oriented Finite Element Programming: Frameworks for Analysis, Algorithms and Parallel Computing: University of California, Berkeley.

[19] T. Okazaki, D. G. Lignos, T. Hikino, and K. Kajiwara, “Dynamic response of a chevron concentrically braced frame,” J. Struct. Eng. (United States), vol. 139, no. 4, pp. 515–525, 2013.

[20] Filippou, F. C., E. P., & Bertero, V. V. (1983), Effects of Bond Deterioration on Hysteretic Behavior of Reinforced Concrete Joints, Earthquake Engineering Research Center, University of California.

[21] P. E. E. R. C. PEER, “PEER Ground Motion Database,” Shallow Crustal Earthquakes in Active Tectonic Regimes, NGA-West2, 2013. [Online]. Available: http://ngawest2.berkeley.edu/.

[22] V. V Bertero, “Strength and deformation capacities of buildings under extreme environments,” Struct. Eng. Struct. Mech., vol. 53, no. 1, pp. 29–79, 1977..

[23] D. Vamvatsikos and C. Allin Cornell, “Incremental dynamic analysis,” Earthq. Eng. Struct. Dyn., vol. 31, no. 3, pp. 491–514, 2002.

[24] J. Coleman and E. Spacone, “Localization issues in force-based frame elements,” J. Struct. Eng., 2001.

[25] E. Karamanci and D. G. Lignos, “Computational approach for collapse assessment of concentrically braced frames in seismic regions,” J. Struct. Eng. (United States), vol. 140, no. 8, 2014.

[26] FEMA-350, “Recommended Seismic Design Critria for New Steel Moment-Frame Buildings Fema 350,” FEMA-350, Washington, DC, 2000.

[27] FEMA-351, “Recommended Seismic Evaluation and Upgrade Criteria for Existing Welded Steel Moment-Frame Buildings, prepared for the Federal Emergency Management Agency,” FEMA-351, Washington, DC, 2000.

[28] Federal Emergency Management Agency (FEMA) P-695, Quantification of building seismic performance factors. 2009.

[29] FEMA P-58-3, “Seismic Performance Assessment of Buildings, Volume 3 - Supporting Electronic Materials and Background Documentation, Third Edition,” 2012. [Online]. Available: https://femap58.atcouncil.org/.

VITA

Mesut Adalı graduated from Ahmet Avcı Anatolian Teacher High School in 2013 and started his training for the Bachelor of Science degree in Civil Engineering at Yıldız Technical University (YTU).

After graduating from YTU with a high honour degree, he started his master studies in Özyeğin University in 2018. His research is focused on the seismic evaluation of chevron braced frames, post-buckling behaviour of steel braces. During his studies, he subsequently worked as a Teaching Assistant in the Civil Engineering Department of Özyeğin University.